Geoarchaeology

WILEY

Geoarchaeology An International Journal

RESEARCH ARTICLE OPEN ACCESS

A Millennium of Coastside Occupation. Micromorphological Insights From the Indigenous Site of Las Estacas Cave, Tenerife

Pedro García-Villa[1,2] | Cristo M. Hernández[1,2] | Carolina Mallol[1,2,3]

[1]Archaeological Micromorphology and Biomarkers Laboratory (AMBI Lab), Instituto Universitario de Bio-orgánica Antonio González (IUBO-AG), Universidad de La Laguna, Canary Islands, Spain | [2]Área de Prehistoria, Departamento de Geografía e Historia, Facultad de Humanidades, Universidad de La Laguna, Canary Islands, Spain | [3]Interdisciplinary Center for Archaeology and the Evolution of Human Behavior (ICArEHB), Universidade do Algarve, Faro, Portugal

Correspondence: Pedro García-Villa (pgarciav@ull.edu.es)

Received: 7 February 2026 | **Revised:** 29 March 2026 | **Accepted:** 30 April 2026

Scientific Editor: Susan Mentzer

Keywords: Canary Islands | coastal archaeology | geoarchaeology | human activities | Island archaeology | site formation | sodic soils

ABSTRACT

The archaeological site of Las Estacas Cave (NW Tenerife, Canary Islands) preserves some of the earliest human occupations in Tenerife, dating to the 2nd century CE, spanning the entire pre-European time range up to the 15th century. Using soil micromorphology, this study applies a geoarchaeological approach to reconstruct site formation processes and human activities through the analysis of 12 thin sections from 9 stratigraphic units, covering most of the sequence. The deposit is largely geogenic and consists of autochthonous basalt fragments, detrital volcanic gravel, and aeolian quartz grains from the Sahara Desert in a spongy clayey matrix characteristic of sodic coastal soils. Aridification evidence in the soil is observed from Unit IV onwards, spanning roughly from the 11th to 15th century. Certain stratigraphic Units (VIII, VII, IV, and II) exhibit increased concentrations of microscopic anthropogenic particles and clear evidence of sedimentary reworking due to trampling. The dominance of geogenic sedimentation and sporadic anthropogenic signals implies episodic use of the cave rather than continuous occupation. The results highlight the interplay between natural depositional processes and human activities in shaping the cave's archaeological record. This study demonstrates the value of microstratigraphic, microcontextual approaches for understanding coastal indigenous sites in Tenerife.

1 | Introduction

The Canarian Archipelago (Figure 1) consists of eight inhabited islands and several uninhabited islets of volcanic origin. Their geological formation is still discussed, with some scholars advocating for a hotspot formation process, similar to Hawaii and Galápagos (Troll and Carracedo 2016b), while others propose a plate-based hypothesis (Anguita et al. 2025).

The earliest known human presence in the Canary Islands is a Roman purpure extraction site in the Islet of Lobos, dated between the first century BCE and the first century CE (del Arco et al. 2016). However, the islands were not settled by the Romans, who appear to have visited the archipelago sporadically for resource extraction. Instead, the Canaries were peopled by Northwest African Berber (Tamazight-speaking) populations who arrived and spread throughout the archipelago between the second and fourth centuries CE, as indicated by chronometric, linguistic, and genetic data (Flores et al. 2001; Fregel et al. 2019; Mora 2021; Morales et al. 2023; Santana et al. 2024; Serrano et al. 2023; Springer 2015). Distinct Aboriginal cultures developed independently on each island for

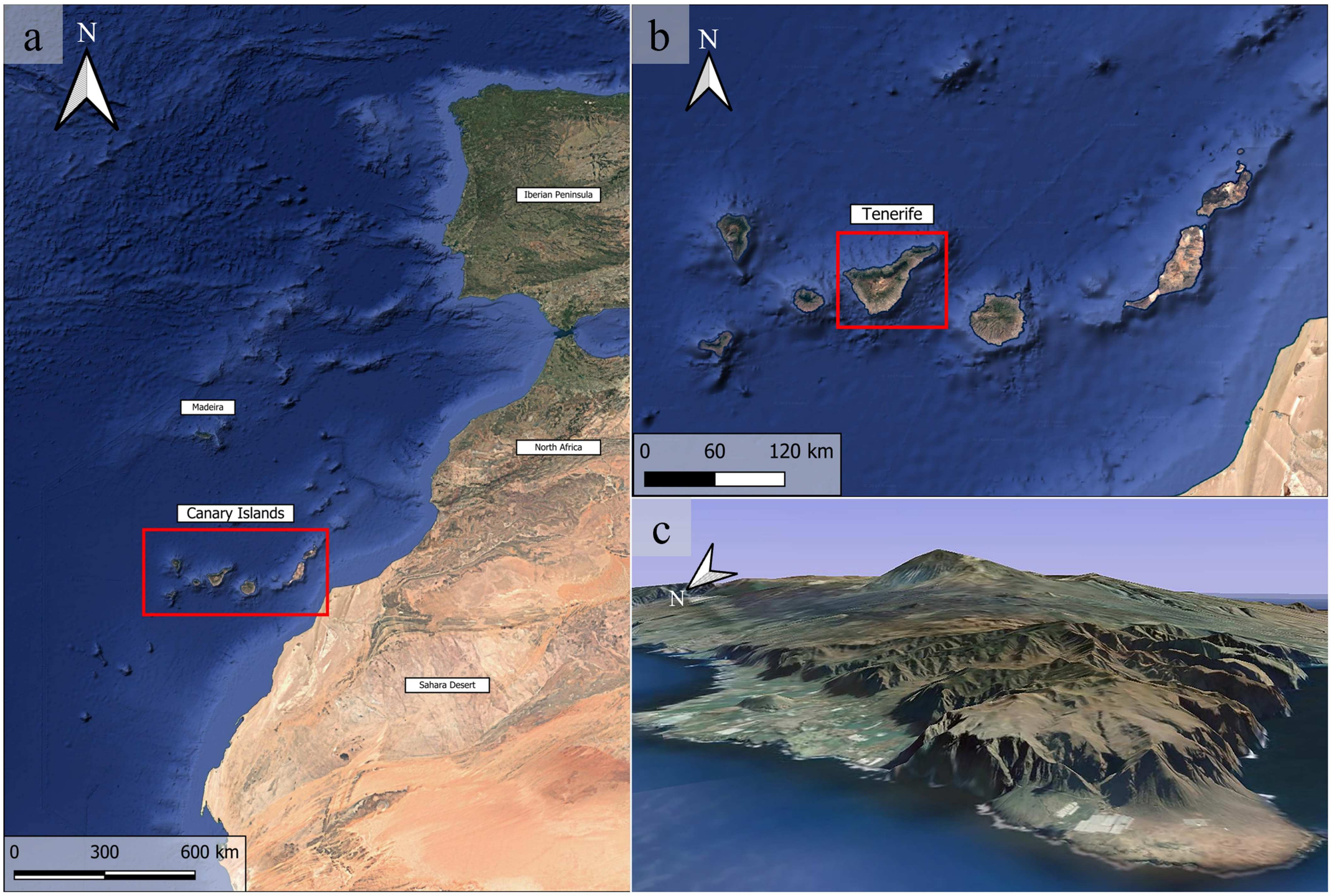

FIGURE 1 | (a) Location of the Canary Islands in relation to NW Africa and the Iberian Peninsula. (b) Location of Tenerife in the Canarian Archipelago. (c) Aerial view of the La Isla Baja and the Teno Massif, where Las Estacas Cave is located. Taken from Figure 19 of Hernández et al. (2024).

ca. 1200–1400 years, until the arrival of Europeans in the 14th and 15th centuries. A recent age model based on radiocarbon dates from Las Estacas Cave in Buenavista del Norte, Tenerife (Hernández et al. Forthcoming), corroborates this timeframe after re-evaluating previous dates from the site (Galván et al. 1999), identifying it as one of the oldest in the archipelago.

Characterizing the cultural adaptations made by the first Canarian settlers as they confronted unfamiliar ecosystems is a complex and compelling area of research. These pioneers faced the challenge of living in an environment with no native mammals or cultivars other than those they brought with them, encountering unknown plants for their animals and unknown soils for their crops. Microstratigraphic geoarchaeology offers valuable tools for this line of inquiry, providing insights into various aspects of the islands' natural ecosystems preserved within the sedimentary record of early Aboriginal archaeological sites. Furthermore, by examining stratified archaeological sequences at small time scales, researchers may uncover evidence of environmental or cultural changes that can deepen our understanding of the cultural evolution of the Canarian Aboriginal population. For example, Gómez et al. (2014) described site formation processes at the site of Fiquinineo—Peña de las Cucharas, in Lanzarote, identifying indigenous occupation events and abandonment periods inside a domestic structure. In the island of Gran Canaria, Herrera-Herrera et al. (2024) identified the use of sheep dung as a construction material used as a flooring material at the site of La Fortaleza de Tirajana during the first centuries of settlement on the island, pointing to endogenous or imported architectural know-how. Rodríguez et al. (2021) analyzed sedimentological features of combustion structures from the Las Dunas de Maspalomas site, in Gran Canaria. Fernández-Palacios et al. (Forthcoming), Fernández-Palacios et al. (2023a, 2023b) described site formation processes at Belmaco and Buracas caves, in La Palma, identifying long-term sheep stables that help approach the pastoralist economy of the island's indigenous population through the centuries. Lastly, Tomé et al. (2022) described the site formation processes and fuel management behaviors of the indigenous occupants of the Roques de García Rockshelter in Tenerife, located at more than 2000 m.a.s.l., and showed evidence for recurrent occupation episodes and use of woody fuel that is not naturally present in the area today.

In this paper, we present the results of a microstratigraphic study using soil micromorphology to characterize depositional and postdepositional processes in the sedimentary sequence of Las Estacas Cave (Figure 2), which spans 1400 years, from the times of the earliest settlers to the arrival of the first European colonizers. Our objective is to provide data on environmental conditions and to assess stratigraphic continuity across the sequence, together with the nature and intensity of human

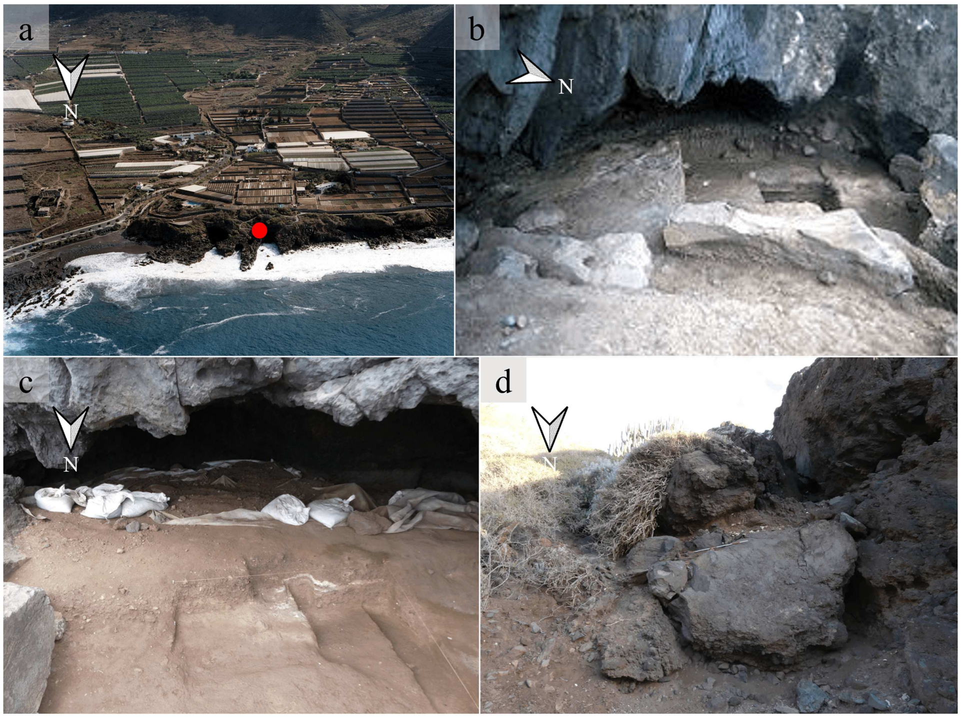

FIGURE 2 | View of Las Estacas cave and its surroundings. (a) Coastline view looking South. The red dot represents the location of the cave. (b) 1990s photograph of the cave site showing the excavation surface and survey. Taken from Galván et al. (2018). (c) Photograph from 2018, when the old profiles were exposed. (d) Fallen megablock with adhering, intact archaeological sediment found a few meters downhill from the cave entrance (towards the ocean front).

activity at the cave entrance. In doing so, this study will contribute to our understanding of the dynamics of the indigenous communities in northwestern Tenerife, where Las Estacas Cave plays a crucial role.

1.1 | Geological Setting of the Study Area

The archaeological site of Las Estacas is located in Buenavista del Norte, northwest of Tenerife, within a coastal platform formed by successive lava deltas known as La Isla Baja (Figure 3). This geographical formation dates to the late Pliocene and Holocene, specifically after the Bruhnes-Matuyama polarity reversal (< 690 kya BP) (Carracedo 1979). To the north, it reaches directly to the Atlantic Ocean; to the south, it is bordered by the Teno Massif, one of the oldest geological structures of Tenerife, with an estimated age of 7.2–5.3 million years (Abdel-Monem et al. 1972; Troll and Carracedo 2016a).

La Isla Baja's formation is closely related to the Teno Massif's development. Initially, the eruptions of Taco and Aregume volcanoes directly from the seabed emitted various trachybasaltic and phonolitic lava flows and pyroclastic deposits, marking the first phase of the lowlands' formation (Descripción de las Unidades Geológicas de Tenerife 2010). Subsequently, three volcanoes located at altitudes exceeding 800 meters in the Teno Massif (La Zahorra or Montaña de El Palmar, Las Portelas Bajas and Las Portelas Altas) erupted, producing mafic basaltic lava flows characterized by their low viscosity. These fluid lava flows channeled through El Palmar Valley, eventually reaching La Isla Baja, where they partially overlapped with earlier emissions, shaping the current shoreline and completing the geological formation of the region. These highly fluid lava flows created numerous caves and volcanic tubes, some of which, including Las Estacas Cave, were used as shelters and living quarters by the indigenous population.

Soil science analyses conducted on the northern shoreline of Tenerife indicate the predominance of vertisols in the lowlands and demonstrate the effects of aridification, salinification, and human activity on soil formation from the 19th century AD onward (Fernández and Tejedor 1975; Fernández et al. 1982; Fernández-Caldas et al. 1980; Tejedor et al. 2009).

Over time, La Isla Baja has experienced profound and irreversible transformations, largely driven by infrastructure expansion and intensive agricultural exploitation. The area's flat terrain, unique within Tenerife, has favored large-scale farming since the early 20th century (Figure 2a). Intensive plowing removed the infertile upper layers of volcanic deposits, which were subsequently replaced with fertile soil transported from the Teno Massif, predominantly andosols. This process, known locally as sorriba (Armas-Espinel et al. 2003; Tejedor et al. 2009), profoundly modified the original geomorphology of the area, leading to the loss of much of the Aboriginal archaeological record. The surviving remains are restricted to the immediate coastal zone and to steep, inaccessible ravines, which, despite the extensive environmental alteration, constitute one of the best-preserved archaeological landscapes on Tenerife. This is evidenced by approximately 35 shell middens recorded in the area (Castilla-Beltrán et al. 2025), as well as by domestic and funerary complexes such as La Fuente, Las Arenas, and Las Estacas (Galván et al. 1991, 1999; Hernández et al. 2024).

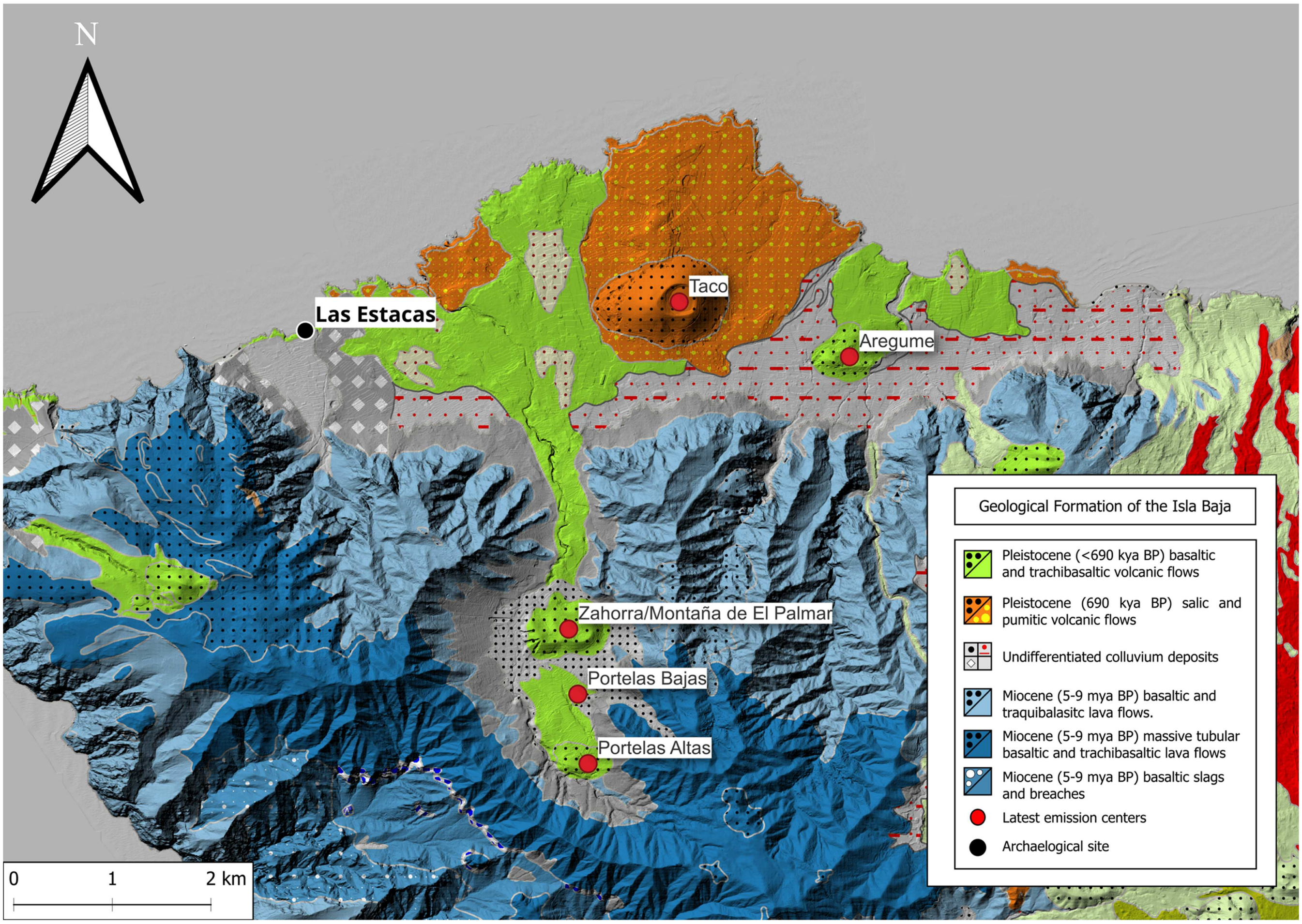

FIGURE 3 | La Isla Baja geological formation, observing the blue geological formation of the Teno Massif and the orange and green representation of the younger volcanic eruptions that formed La Isla Baja. Adapted and modified from GRAFCAN.

TABLE 1 | Field stratigraphic data gathered from the 1990s excavations and the 2018 sampling season. Thickness and absolute dates are taken from Hernández et al. (Forthcoming), while texture and color observations are from Galván et al. (1998).

SU	Thickness	Absolute dates (AD)	Texture	Color	Associated samples	Observations
I	20	1451	Compact fine - Loose granular	5YR 4/2–5YR 3/2	—	Fully excavated
II	8	1329	Very fine	10YR 4/2	Block n° 3	Excavated on the exterior
III	12	1295	Compact fine—Loose granular	5YR 4/3	Block n° 3	Excavated on the exterior
IV	13	1021	Compact very fine—Loose granular	7.5YR 4/2	Block n° 1	Excavated on the exterior
V	6	661	Compact fine—Loose granular	10YR 4/3	Block n° 1	Excavated on the exterior, Major roof spall event
VI	11	598	Fine	10YR 3/3	Block n° 4	Excavated on the exterior, major roof spall event
VII	9	530	Very fine	10YR 5/3	Block n° 2	Excavated on the exterior
VIII	6	463	Very fine	5YR 3/3	Block n° 2	Excavated in a 1 × 1 survey
IX	24	409	Very fine	5YR 4/3	Block n° 2	Excavated in a 1 × 1 survey
X	15	167	Very fine	5YR 3/3—7.5YR 4/3	Block n° 2	Excavated in a 1 × 1 survey
XI	6	76	Very fine	5YR 3/2	—	Excavated in a 1 × 1 survey
XII	—	34	Very fine	2.5YR 4/2	—	Excavated in a 1 × 1 survey

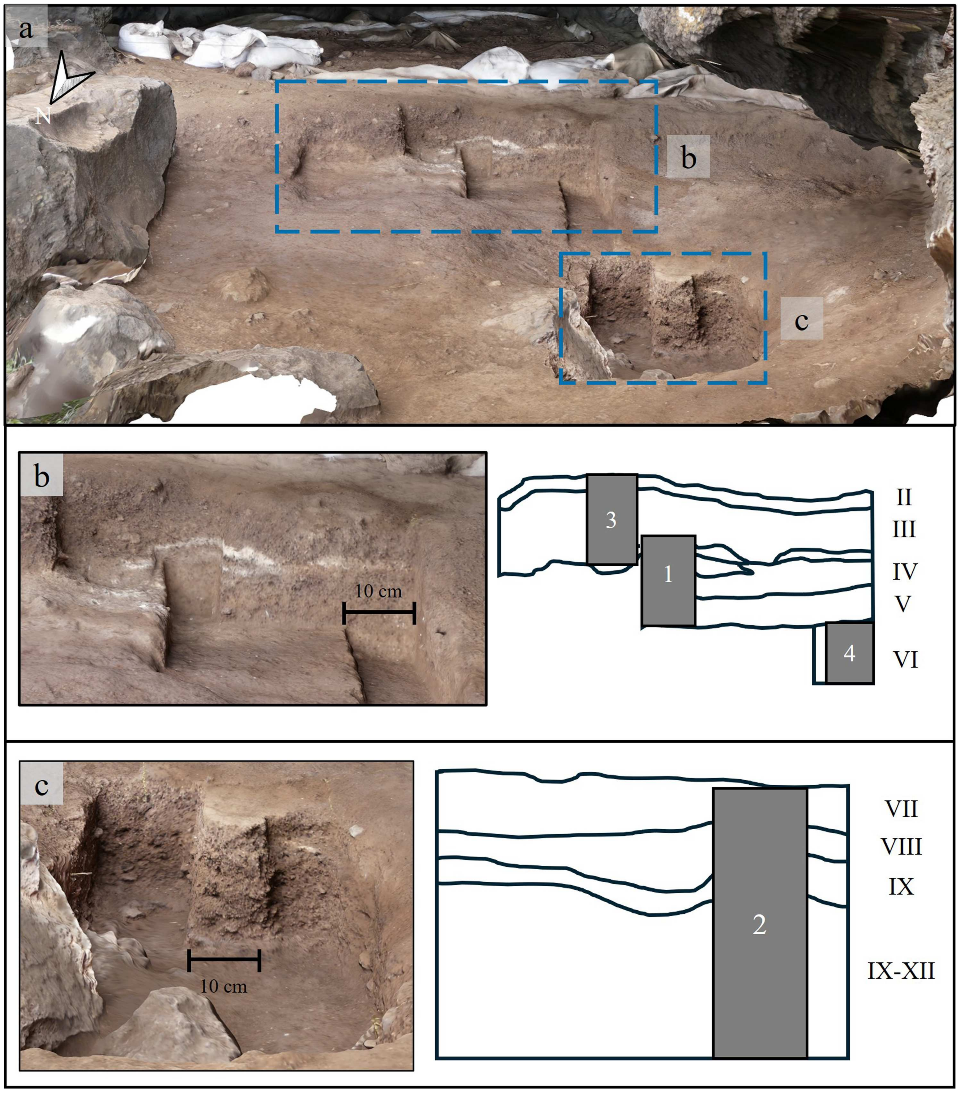

FIGURE 4 | Photogrammetric model of the sampled surface and profiles, Units sampled, and provenance of the micromorphology blocks. (a) Overview of the cave sedimentary deposit and the two profiles recovered from the 1990s excavation during 2018 sampling campaign. (b) Main profile with Units II-VI. (c) 1x1 m survey showing Units VII-XII.

1.2 | Site Background

During the late 1970s and 1990s, the shoreline of the municipal area of Buenavista was subject to intensive archaeological survey and excavation (Galván et al. 1998, 1991, 1999, 2004; Hernández et al. 2024, fig. 18). Various archaeological sites, including funerary, habitational, and shell-midden contexts, were discovered and fully or partially excavated.

These surveys identified two archaeological sites composing the Las Estacas archaeological complex: Las Estacas 1, a 26 m^2 domestic cave, and Las Estacas 2, a 5 m^2 funerary cave. Surface finds in Las Estacas 2 included a scatter of fragmented human remains, underlain by the remains of a reworked young-adult individual. Currently, the two cavities are separated by the modern access path, but they are located ca. 10 m away and are formed by the same lava flow.

Excavations at Las Estacas 1 (hereafter Las Estacas) exposed a stratified sequence of ca. 130–1.50 m that was divided into 12 Stratigraphic Units (SU) (Table 1, Figure 4). Laterally, a distinction was made between an interior and an exterior area based on macroscopic sedimentary features, in situ hearth locations, and the position of the current dripline (Galván et al. 1998). Unit I was excavated entirely, Units VI-II were excavated in the exterior area, and Units VII–XII were excavated in a 1 × 1 m survey, also in the exterior area (see Appendix S1 for a 3D model of the site). The cave opens NE directly to the Atlantic Ocean, with an aperture of 5.10 m. A cornice collapse event is evidenced by the presence of fallen mega blocks between Units VI and V. This collapse resulted in a decrease in the sheltered area. The fall of a mega block also implies a reduction of the habitable area outside the cave, which is small and very close to the coastal cliff. Further evidence of the collapse is located downslope, a few meters from the cave, where a stratified archaeological sedimentary deposit is sandwiched between two fallen mega blocks. This deposit was possibly detached from the surface in front of the cave and transported downslope, coinciding with the cornice-collapse event and further disrupting the original continuity between Las Estacas 1 and 2.

TABLE 2 | Modified and adapted from Galván et al. (1998), indicating the nature and quantities of archaeological materials and features of interest uncovered from the '90 s excavations. Limited data is available for Units XII–IX.

	Archaeological materials and features of interest recovered from the '90s excavations							
SU	**Ch**	**I**	**M**	**TF**	**BD**	**OD**	**Ce**	**CF**
I	1587	326	2980	1971	576	381	370	2
II	240	24	33	129	17	22	1	
III	843	30	104	198	341	112	98	1
IV	421	95	19	121	345	35	33	
V	1931	1015	333	1247	341	45	307	
VI	1105	910	2587	273	127	18	60	4
VII	832	766	2674	131	126	13	57	1
VIII	407	103	55	56	10	3	13	1
IX	No data		19	No data	—	—	1	
X			212		3	—	6	
XI			30		—	—	4	1
XII	Sterile layer							

Abbreviations: BD, Basalt Debitage; Ce, Ceramics; CF, combustion features; Ch, charcoal; I, Ictiofauna; M, Malacofauna; OD, Obsidian Debitage; SU, stratigraphic unit; TF, Terrestrial Fauna.

Numerous archaeological finds (Table 2) were recovered in the excavations of Galván et al. (1998). Faunal remains include those of ovicaprids and suids, as well as sporadic finds of canids, avifauna, and the giant Tenerife lizard *Gallotia goliath*. Malacofaunal remains are mainly from the *Patellidae* family (Mesa 2018), and fishing evidence includes species such as *Sparisioma (Euscarus) cretense* and Murenidae. The lithic industry is composed primarily of basalt tools, with low quantities of obsidian. Several combustion structures were documented, varying in morphology: flat hearths, pit hearths, and stone-lined hearths. Pottery remains include types II-III (Arnay and Reimers 1984) in the lower Units, with an increase in type I pottery from Unit V onwards. Anthracological analyses revealed species from the immediate environment, including *Juniperus turbinata* and *Erica arborea*, as well as high-altitude taxa, such as *Pinus canariensis* (Yanes et al. 2001).

2 | Materials and Methods

Geoarchaeological sampling for this study took place in 2018 over two seasons. The main sections from previous excavations were cleaned back 10 cm, visible features of the stratigraphic sequence and individual Units were described, and samples were collected for soil micromorphology, lipid biomarkers, sclerochronology, pollen, and phytolith analysis.

2.1 | Soil Micromorphology

Four intact and oriented micromorphological blocks were extracted in the 2018 sampling seasons. Samples from Units II–V were collected from a sheltered central zone within the cave, 10 cm inward from the current dripline. The sample from Unit VI was collected approximately below the current dripline, and the samples from Units VII to X were collected from an exposed zone outside the current dripline. Based on a hypothetical position of the dripline prior to the major cornice collapse event that occurred between Units V and VI, all the micromorphology samples represent sediment from sheltered areas of the cave near the dripline, including the ones from Units V–II.

Initial block processing was carried out at the Laboratory for Archaeological Micromorphology and Biomarkers (AMBILAB) at the University of La Laguna. Blocks were heated at 60°C for 48 h and then impregnated with a mixture of unaccelerated polyester resin, styrene monomer, and a catalyst (methyl-ethyl-ketone) at a ratio of 7:3:0.1. Once consolidated, the blocks were cut into ca. 2 cm-thick slabs using a Euro-Shatal M31100 radial saw.

The slabs from two blocks (1 and 3) were further processed by Wagner Petrographics, resulting in eight thin sections of 7.50×5 cm. Slabs from blocks 2 and 4 were processed at the AMBILAB, resulting in four thin sections of 9×6 cm. Slabs were thinned down to ca. 1 mm using a Uniprec ATA Brilliant-220 precision cutting machine, and they were further polished to ca. 30 μm using a G&N MPS-Geology grinding machine. A total of 12 thin sections were analyzed in this study (Appendix S2).

Samples were analyzed using Plane Polarized Light (PPL), Cross Polarized Light (XPL), and blue light under a Nikon E600 POL and a Nikon AZ1000 petrographic microscope. A microfacies approach was employed in the study of the thin sections (Courty 2001), in which layers with different lithology, groundmass, porosity, and anthropogenic inclusions are separated as different microfacies units (MFU), assuming their composition is associated with different depositional or postdepositional processes. Similar MFUs are grouped into microfacies types (MFT) to identify recurring processes along the sequence. Samples were analyzed following the parameters in Stoops (2021) and Nicosia and Stoops (2017).

2.2 | Sediment Deposition Rate

Using the Bacon model of the calibrated dates from Las Estacas (Blaauw and Christen 2011; Hernández et al. Forthcoming), a model of sediment depositional rate (SDR) was calculated, based on the ratio between the thickness of the individual Unit (z_2–z_1) and the corresponding age difference (t_2–t_1), with results expressed in centimeters per year (cm/y). The following equation has been used:

$$\mathrm{SDR} = \frac{z_2 - z_1}{t_2 - t_1}.$$

3 | Results

The archaeosedimentary sequence of Las Estacas cave is characterized by a suite of micromorphological features that are common to all the stratigraphic Units. The groundmass is clayey with unsorted basalt fragments (silt to gravel size) displaying variable degrees of roundness and different frequencies throughout the Units. Generally, the sediment is massive and apedal, except in Units V and III, where peds are partially developed. In these Units, interpedal porosity is characterized by planar voids, while apedal and intra-pedal porosity mainly comprise vughs, along with common vesicles and channels. The main microstructure is spongy and vughy (Figure 5), with a minor presence of channel and vesicular microstructure, where several connected and interconnected vughs dominate the sediments' porosity features. These vughs are often intertwined with the less abundant channels and vesicles. The coarse/fine (c/f) ratio ranges from 30/70 to 60/40. The related distribution is predominantly double-space enaulic in most of the Units and open porphyric in the combustion features. The general b-fabric is grano-porostriated and crystallitic in the combustion features (see Appendix S3 for a detailed description of soil characteristics and components).

Regarding lithology, the basalt fragments throughout the sequence, which are commonly variably angular to rounded, and silt-to-sand-sized except in Units III, X, and IV, where they are gravel-sized, exhibit porphyric textures with a microcrystalline matrix rich in plagioclase and magnetite, along with olivine and augite phenocrystals. Sometimes phenocrystals are loose in the sediment. All-rounded, subrounded basalt fragments exhibit high porosity and contain clay inclusions. Small amounts of rounded, sand-sized vesicular basalt fragments, trachybasalts, and phonolites are also present throughout the deposit. Additional lithological elements include common fine silt-sized, subrounded quartz grains.

The natural and anthropogenic coarse fraction (Figure 6) includes fragments of rounded-subrounded and angular basalt (Figure 6a,b), charcoal (Figure 6c,d), plant remains, amorphous organic matter, dung, bone, ceramic (Figure 6e,f), and limpet shells (Figure 6g,h), all of which vary in size, abundance, and preservation state. Calcite pseudomorphs after calcium oxalate crystals characteristic of wood ash are present alongside fecal spherulites and opaline phytoliths, all displaying varying degrees of preservation in Units VIII, IV, and III, and are directly associated with combustion features and wood ash deposits (Appendix S3). Authigenic evaporitic minerals are found in Units IV and III. Three different in situ combustion structures have been identified. Combustion Structure 1 (CS1) is in Unit VIII and overlays MFU 3 and MFT 3. Combustion Structure 2 (CS2) in Unit IV overlays MFUs 15–17 and MFTs 7 and 8, and Combustion Structure 3 (CS3) is also in Unit IV and overlays MFUs 18–20 and MFT 9. A patch of reworked calcitic wood ash (MFT 11–MFU 24) was identified in Unit III.

Pedofeatures (Figure 7) found in all the Units include abundant textural features, such as microlaminated limpid infillings, clay coatings, and hypocoatings (Figure 7a–d) around pores and coarse elements, along with a few typic and concentric Fe-Mg-rich anorthic nodules. These are predominantly abundant in

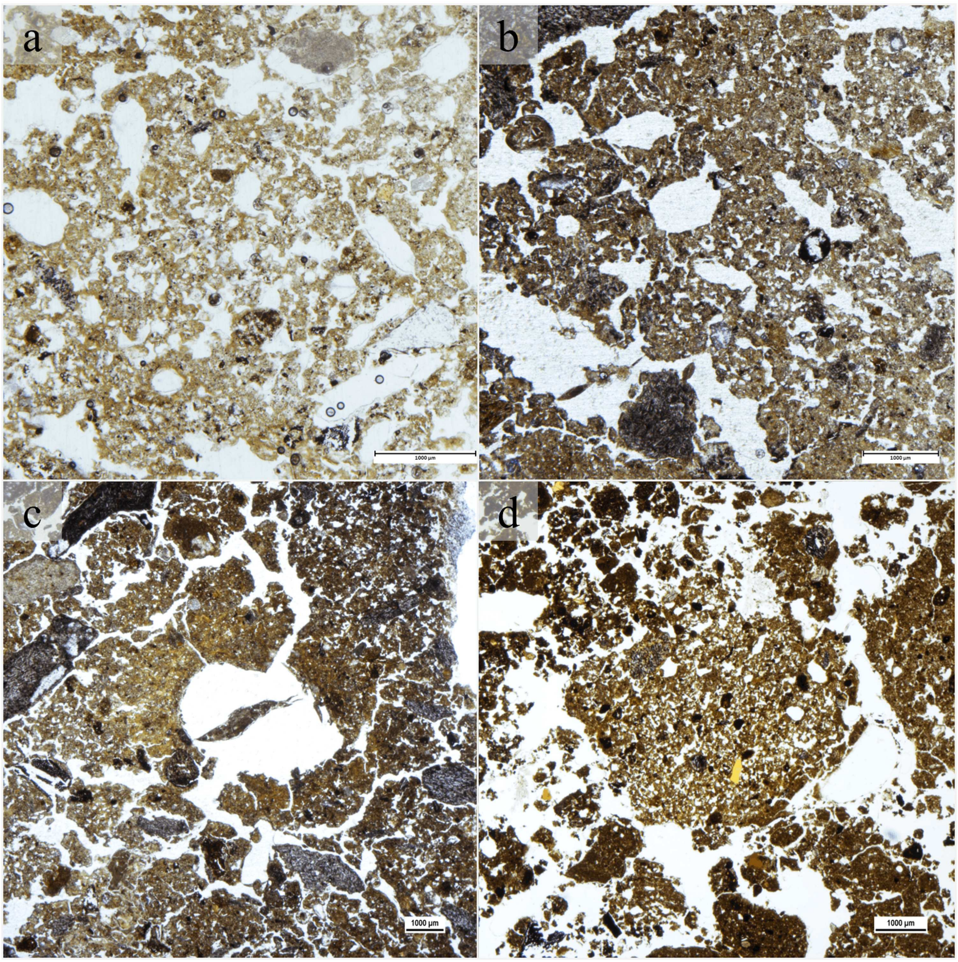

FIGURE 5 | Spongy vertisol features: (a, b) Spongy microstructure with abundant star-shaped vughs, channels, and vesicles. PPL, Unit X. (c) Spongy microstructure with a central channel. Note the compaction around the channel's edges and the plant matter fragment in its interior, PPL, Unit IX. (d) Vughy soil aggregate, with a bone fragment. PPL, Unit VII.

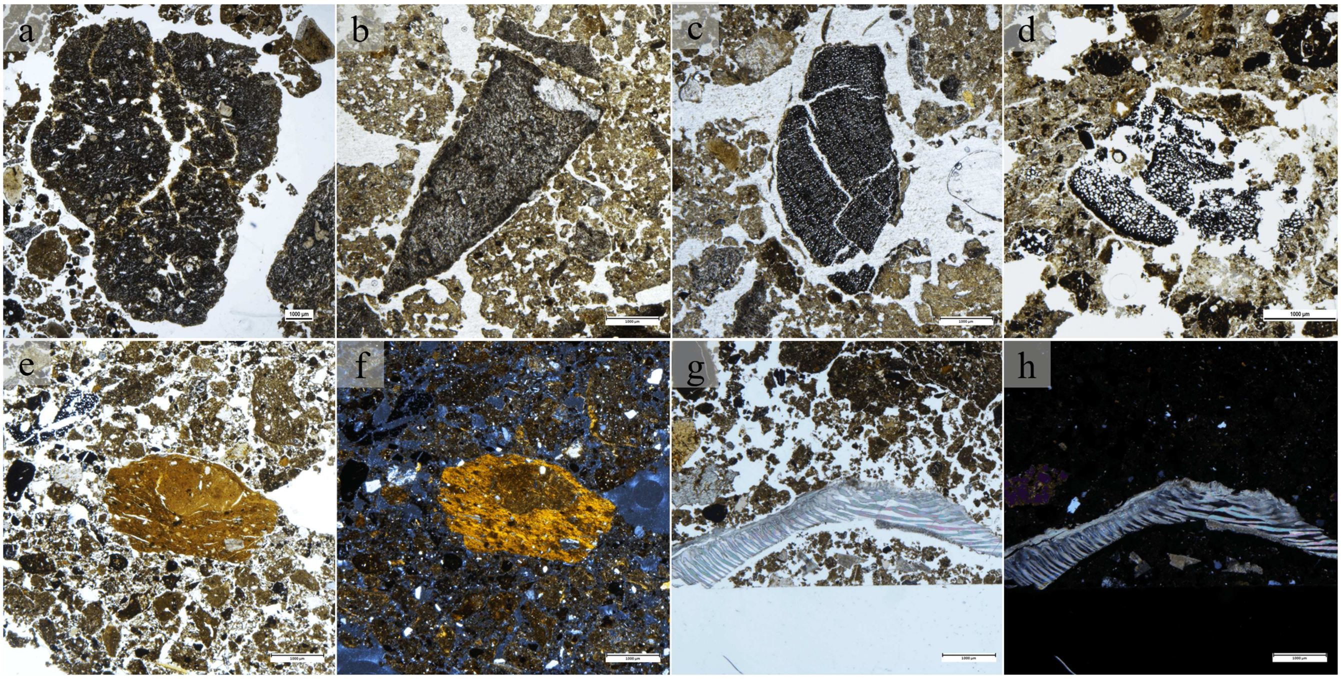

FIGURE 6 | Main natural and anthropogenic sand and gravel-sized components: (a) Subrounded-rounded weathered basalt, PPL, Unit III. (b) Angular basalt, PPL, SU X. (c, d) Subrounded charcoal, PPL, Unit X. (e, f) Low-temperature fired subrounded ceramic fragment, PPL-XPL, Unit III. (g, h) Un-heated aragonitic shell fragment (limpet), PPL-XPL, Unit VII.

Units X–V, with a slight decrease in abundance in Units IV–II. In Units VIII, VII, and V there are fragments of sedimentary surface crusts (Pagliai and Stoops 2010) composed of successive layers of sand, silt, and clay (Figure 7e–h). These are present as in situ fragments and rip-up clasts.

Based on the abundance and features of the soil components and materials, 25 MFUs have been identified and categorized into 12 different MFTs. See Appendix S2 for a visual differentiation of each MFU and Appendix S3 for a detailed description of each component of the MFU.

3.1 | Human Activity

Compared to the macroscopic archaeological record recovered during the excavations of Units XI–I at Las Estacas (Galván et al. 1998), the microscopic anthropogenic record examined here is notably sparse and concentrated mainly in Units VII, IV, and III. Throughout the sequence, the microscopic anthropogenic remains consist of scattered subangular charcoal fragments, shell fragments showing various degrees of thermal alteration, very few bones, and very few ceramic fragments in Units III, IV, and IX. The most distinct evidence of human activity is located in the top of Units III, Unit VII, and several remains of combustion activity in Units VIII and IV (Table 3).

Stratigraphic Unit VII is composed of a series of loose aggregates characterized by a dominant complex packing-void microstructure and secondary channels (Figure 8). Aggregates possess a variable composition and microstructure, ranging from limpid clay aggregates (Figure 8b,c), clayey surface crusts rip-ups (Figure 8d), silt-sized grained aggregates (Figure 8e), aggregates with archaeological materials, like bone, shell, and charcoal (Figure 8f–g), and with sodic soil features (Figure 5d).

Unit III is capped by a massive deposit composed of thermally altered sodic soil aggregates and reworked calcitic wood ash, with no primary porosity (Figure 8h,i). Secondary porosity is limited to postdepositional root bioturbation channels.

Primary combustion activity was observed in Unit VIII (CS1) and in Unit IV (CS2 and CS3). These features differ in composition and preservation. CS1 consists of a black layer composed of silt and fine sand-sized charred plant matter and charcoal in a clayey geogenic groundmass. The black layer is capped by two sedimentary surface crusts. The lower crust (MFU 4), 2–3 mm-thick, is fragmented, and the top one (MFU 5), 4–6 mm thick, is crossed by a 1 cm-thick layer of recrystallized wood ash.

The two combustion structures in Unit IV, CS2 and CS3, occur throughout the Unit, and their substrates show spongy soil properties. The substrate of CS2 consists of a 1–2 m-thick red layer overlain by a 5.5–6 cm-thick calcitic wood ash deposit (Figure 9). This ash deposit contains well-preserved calcite pseudomorphs after calcium oxalate and subangular to rounded, unsorted rubified clay aggregates, which are common in MFU 16 and abundant in MFU 17 (Figure 9a,b). No charcoal fragments were identified. The CS2 ash layer also includes a segment of possible sintered and crusted ash (Karkanas 2021), particularly in MFU 16 (Figure 9c–f). In MFU 17, where rubified clay aggregates are most abundant, no sintered or crusted ash was observed.

CS3 exhibits a markedly different composition from CS2 (Figure 10a). It consists of a mixture of clay aggregates,

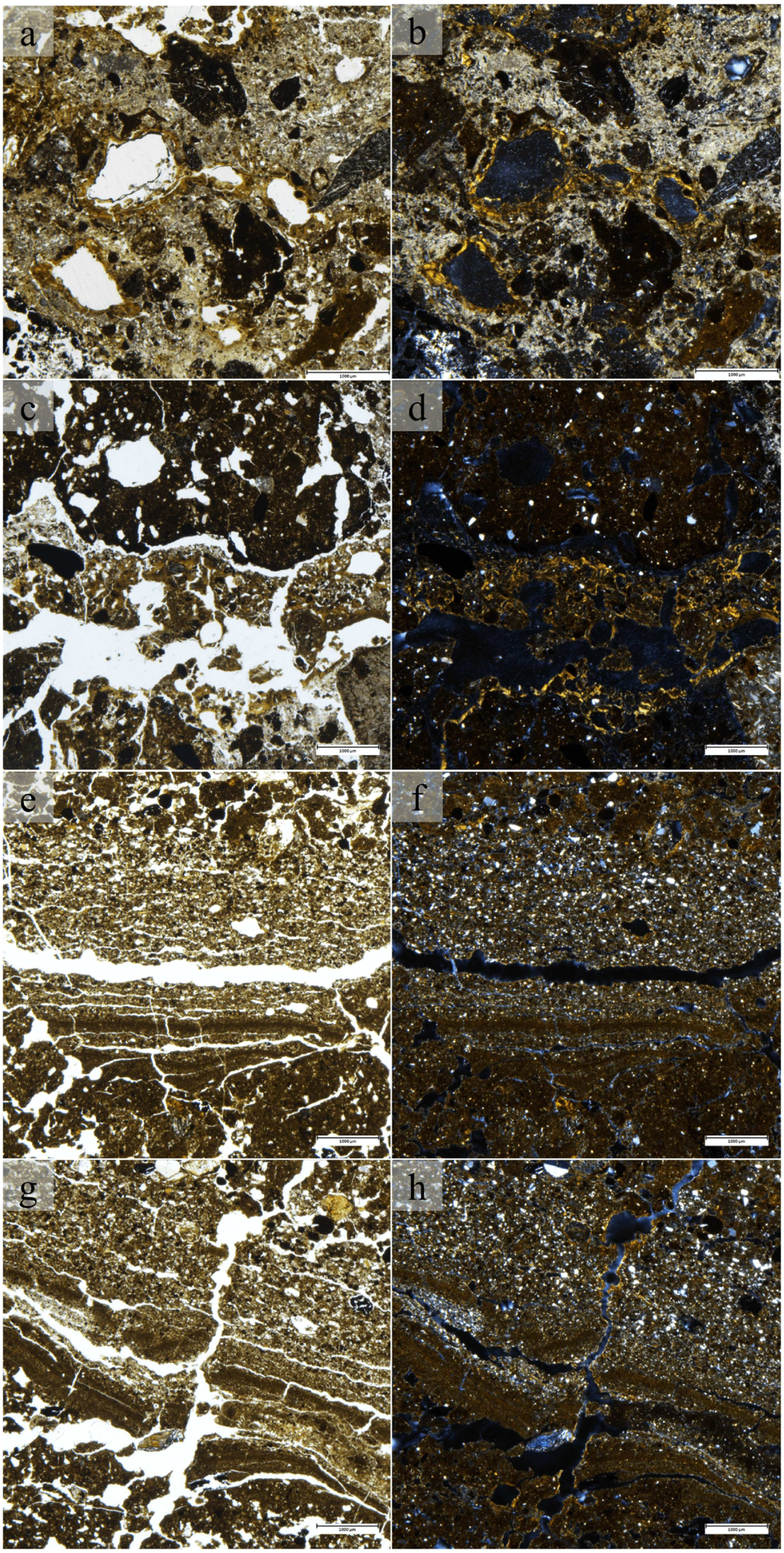

FIGURE 7 | General and specific pedofeatures found in Las Estacas archaeosedimentary sequence: (a, b) Clay coatings in an ashy matrix, PPL-XPL, Unit III. (c, d) Clay infillings in a channel, PPL-XPL, Unit III. (e–h) Surface crusts. Note the bedded succession of sand—silt and clay particles, indicating the presence of still water.

TABLE 3 | Description of each MFT included in this study.

MFT	MFU	SU	Description	Interpretation
1	1, 23	X, III	Clayey groundmass with abundant angular gravel- and sand-sized basalt fragments and subrounded silt-sized quartz grains. Sodic soil features: spongy microstructure with dominant vughs, secondary channels, and vesicles, and very few evaporitic crystals in Unit III. The C/F related distribution is double-space enaulic, and the b-fabric is poro-grano striated. Archaeological remains are scarce, including scattered charcoal fragments.	Poorly developed sodic vertisol.
2	2, 9, 22, 25	IX, VI, III	Clayey groundmass with common rounded sand-sized basalt fragments and subrounded silt-sized quartz grains. Sodic soil features: spongy microstructure with dominant vughs, secondary channels, and vesicles, and very few evaporitic crystals in Unit III. The C/F related distribution is double-space enaulic, and the b-fabric is poro-grano striated. Archaeological remains are scarce, including scattered charcoal fragments.	Poorly developed sodic vertisol.
3	3	VIII	Organic-rich (silt-sized black organic particles) clayey groundmass with coarse sand-sized rounded basalt fragments and subrounded silt-sized quartz grains. Sodic soil features: spongy microstructure with dominant vughs, secondary channels, and vesicles. The C/F related distribution is double-space enaulic, and the b-fabric is poro-grano striated. Frequent root remains are observed inside the channels. Charcoal fragments are common.	Poorly developed sodic vertisol and Combustion Structure 1 (Black Layer)
4	4, 5, 11, 13, 14, 15	VIII, VII, V	Clayey lenses exhibiting inverse bedding with a succession of sand, silt, and clay laminations, found in situ in Units VIII and V and as rip-up clast aggregates in Unit VII. Archaeological remains are absent.	Sedimentary surface crust
5	6,7,8	VII	Loose aggregates with a dominant complex packing void microstructure and secondary channels. Variable composition and microstructure: (1) clayey with sodic soil features (spongy microstructure with dominant vughs, secondary channels, and vesicles), (2) 1 with silt-sized particle inclusions, (3) clayey surface crust rip-ups clasts, (4) 1 with bone, shell, and charcoal fragments, and surface crust rip-ups. Sodic soil features: spongy microstructure with dominant vughs, secondary channels, and vesicles. Common scattered archaeological remains, including malacofauna, fine sand charcoal, and bone fragments.	Trampled surface.
6	10, 14	V, IV	Clayey groundmass with few rounded-subrounded gravel-sized basalt fragments, loose sand-sized volcanic phenocrysts, and subrounded silt-sized quartz grains. Sodic soil features: spongy microstructure with dominant vughs, secondary channels, and vesicles with a weakly developed pedality. The C/F related distribution is double space enaulic and the b-fabric is poro-grano striated. Surface crusts are common in Unit V, while absent in Unit IV. Archaeological remains are absent.	Weakly developed sodic vertisol with evidence of stagnant water
7	15	IV	Clayey groundmass with few rounded-subrounded gravel-sized basalt fragments and subrounded silt-sized quartz grains. Sodic soil features: spongy microstructure with dominant vughs, secondary channels, and vesicles with a weakly developed pedality. The C/F related distribution is double space enaulic and the b-fabric is poro-grano striated. The top mm of the layer is rubified. Archaeological remains are absent.	Red layer of Combustion Structure 2
8	16, 17	IV	Calcitic-groundmass with abundant rubified, rounded, sand-sized clayey aggregates. Abundances of rounded sand-sized clay aggregates are higher in MFU 17 than in MFU 16. Microstructure is granular/	White layers of Combustion Structure 2

(Continues)

TABLE 3 | (Continued)

MFT	MFU	SU	Description	Interpretation
			massive with dominant vughs and channels. The C/F related distribution is porphyric and the b-fabric is calcitic crystallitic. Archaeological materials are absent.	
9	18, 19, 20	IV	Groundmass composed of a mixture of herbivore coprolites, calcitic wood ash, clay with common rounded sand-sized basalt fragments, and a few evaporitic crystals and subrounded lime-sized quartz grains. The sediment possesses a complex microstructure, with loose areas characterized by a packing void microstructure and other areas with a massive clayey microstructure. Porosity includes dominant channels, secondary planes, and vesicles. The C/F related distribution is double-space enaulic, and the b-fabric is poro-grano striated. Archaeological remains are abundant, including common unburnt, rubified, and charred dung, and a few fecal spherulites, common charcoal fragments, and a few rubified bone fragments.	Combustion Structure 3.
10	21	III	Clayey groundmass with very abundant gravel-sized rounded basalts and subrounded lime-sized quartz grains. Sodic soil features: spongy microstructure with dominant vughs, secondary channels, and vesicles, and very few evaporitic crystals. The C/F related distribution is double-space enaulic, and the b-fabric is poro-grano striated. Archaeological remains are absent.	Weakly developed sodic vertisol with a series of high-energy deposition events.
11	24	II	Clayey and crystallitic groundmass composed of a mixture of clay aggregates and secondary ash aggregates with common rounded sand/silt-sized basalts and subrounded lime-sized quartz grains. The sediment possesses a sodic spongy microstructure with porosity features dominating vughs and channels, and secondary vesicles. The C/F related distribution is double-space enaulic, and the b-fabric is poro-grano striated and crystallitic. Archaeological materials are scattered, including charcoal, burnt bones, and ceramic fragments.	Sweeping inside the cave—waste disposal.

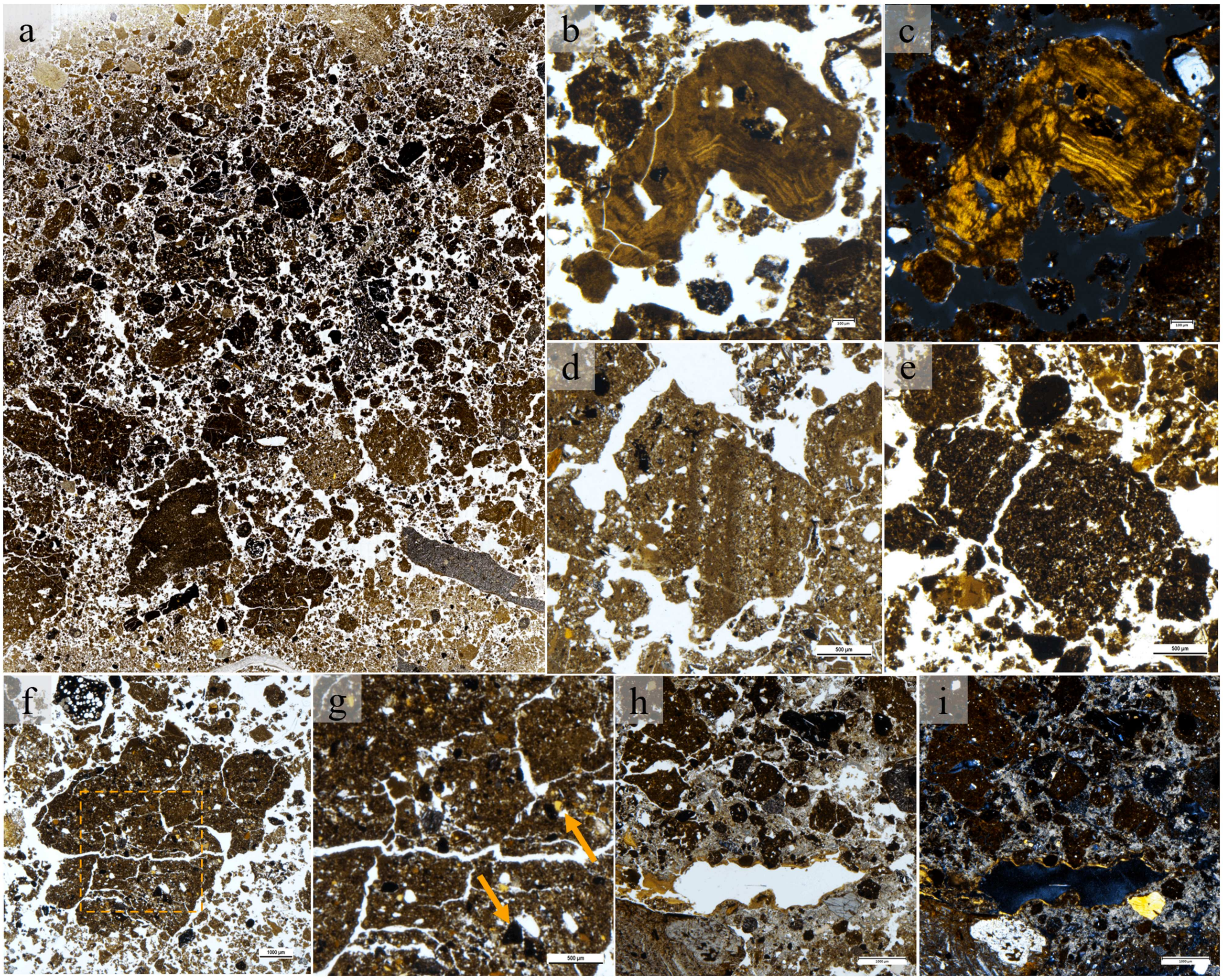

FIGURE 8 | Stratigraphic Unit VII. (a) PPL scan of thin section EST-18-2a, Unit VII, PPL. Note the loose state of the sediment, with complex packing voids and unsorted aggregates of different composition from trampling under dry conditions (Gé et al. 1993). Thin section size: 4.5 × 5.5 cm, PPL, Unit VII (b, c) Limpid clay papule, PPL-XPL, respectively, Unit VII. (d) Surface crust rip-up fragment, PPL, Unit VII. (e) Aggregate derived from a trampled occupation surface, PPL, Unit VII. (f) Aggregate derived from a trampled occupation surface containing fine-sand-sized bone and charred organic fragments. The orange square represents the image area in g) PPL; Unit VII. (g) Magnification of aggregate with orange arrows indicating the silt-sized bone and charred organic fragments. PPL, Unit VII. (h–i) Calcitic Wood ash mixed with sodic soil aggregates and basalt fragments. PPL and XPL, respectively, Unit III.

herbivore dung aggregates, wood ash, charcoal, and shell fragments in various states of thermal alteration (Figure 10b,c). The three MFUs that compose this combustion feature contain the same components, but MFUs 18 and 20 show an open porosity. The dung aggregates appear unaltered, rubified, or charred (Figure 10d–g), with variable fecal spherulite preservation depending on the degree of thermal alteration (Figure 10h,i).

3.2 | Sedimentary Depositional Rate Model

The results from the SDR model are shown in Table 4. SDR ranges from 0.036 cm/year (Unit IV) to 0.235 cm/year (Unit II), with an overall average of 0.130 cm/year. Units I, V, VI, VII, VIII, IX, X, and XI exhibit a relatively consistent rate, between 0.095 and 0.165. Units that deviate from this average include Unit II, with an SDR of 0.235 cm/year, and Units III and IV, with 0.044 and 0.036 cm/year, respectively. These Units correspond to the changes in the cave's morphology and to a chronological discontinuity within the dated sequence.

4 | Discussion

4.1 | Natural Depositional Processes

The geogenic sedimentary components found in the cave's deposit are both autochthonous and allochthonous, as inferred from their angularity and lithological nature. The unsorted, angular basalt clasts derive from natural degradation of the cave ceiling and walls, as they match the lithological description of the lava flow where the cave is located (Descripción de las Unidades Geológicas de Tenerife 2010). Their presence throughout the sequence indicates that this was a continuous process over time, rather than being confined to specific periods.

Allochthonous components include clay, unsorted, subrounded silt-sized quartz grains, and unsorted, rounded-subrounded

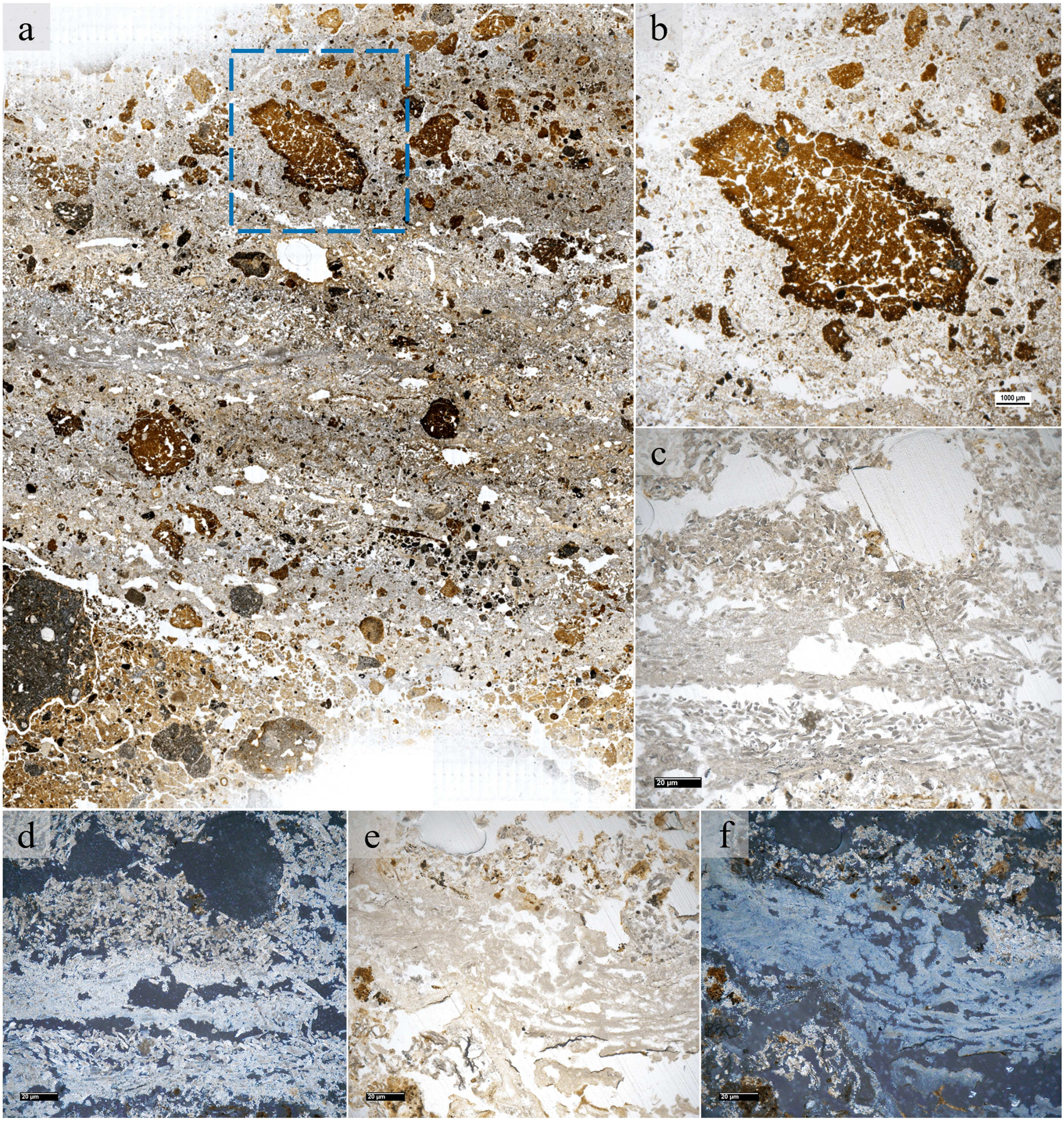

FIGURE 9 | CS 2 (Unit IV): in-situ ash deposits with burnt clay aggregates. (a) PPL scan of thin section EST-18-1-2b, CS 2, Unit IV. Note the abundance of calcitic wood ash and the absence of charcoal, bone, or any other material besides burnt, rounded soil-sediment aggregates. Thin section size: 4.5 × 5.5 cm. The blue square represents the augmented image area in b), PPL, Unit IV (b) Close-up of the rounded aggregates. The larger ones exhibit vughy microstructure and *in situ* burning affecting the outer mm of the aggregate. In XPL, the burnt outer rim exhibits a lower birefringence than the interior, indicative of burning. (c,d) Succession of in-situ wood ashes and possible “crusted ashes,” sensu Karkanas (2021). (e,f) Layer of possible sintered wood ash showing lower birefringence (top half of the image), which indicates temperatures > 900°C, PPL and XPL, respectively, Unit IV.

sand-to-gravel-sized, variably weathered basalt fragments. The quartz silt-sand is windblown from Africa. It is a typical component of sedimentary deposits in the Canary Islands, locally known as *calima* (Menéndez et al. 2007; Mizota and Matsuhisa 1995; Muhs et al. 2019; von Suchodoletz et al. 2013). Aeolian processes play a key role in the sedimentary environment of Las Estacas due to the persistent Easterly trade winds (*vientos alisios*). These year-round air currents, which blow predominantly from the northeast across the Canary Islands, align with the cave entrance, which also faces NE. As a result, the constant winds act as a significant source of detrital silt-sized particles that are transported into and subsequently trapped within the cave.

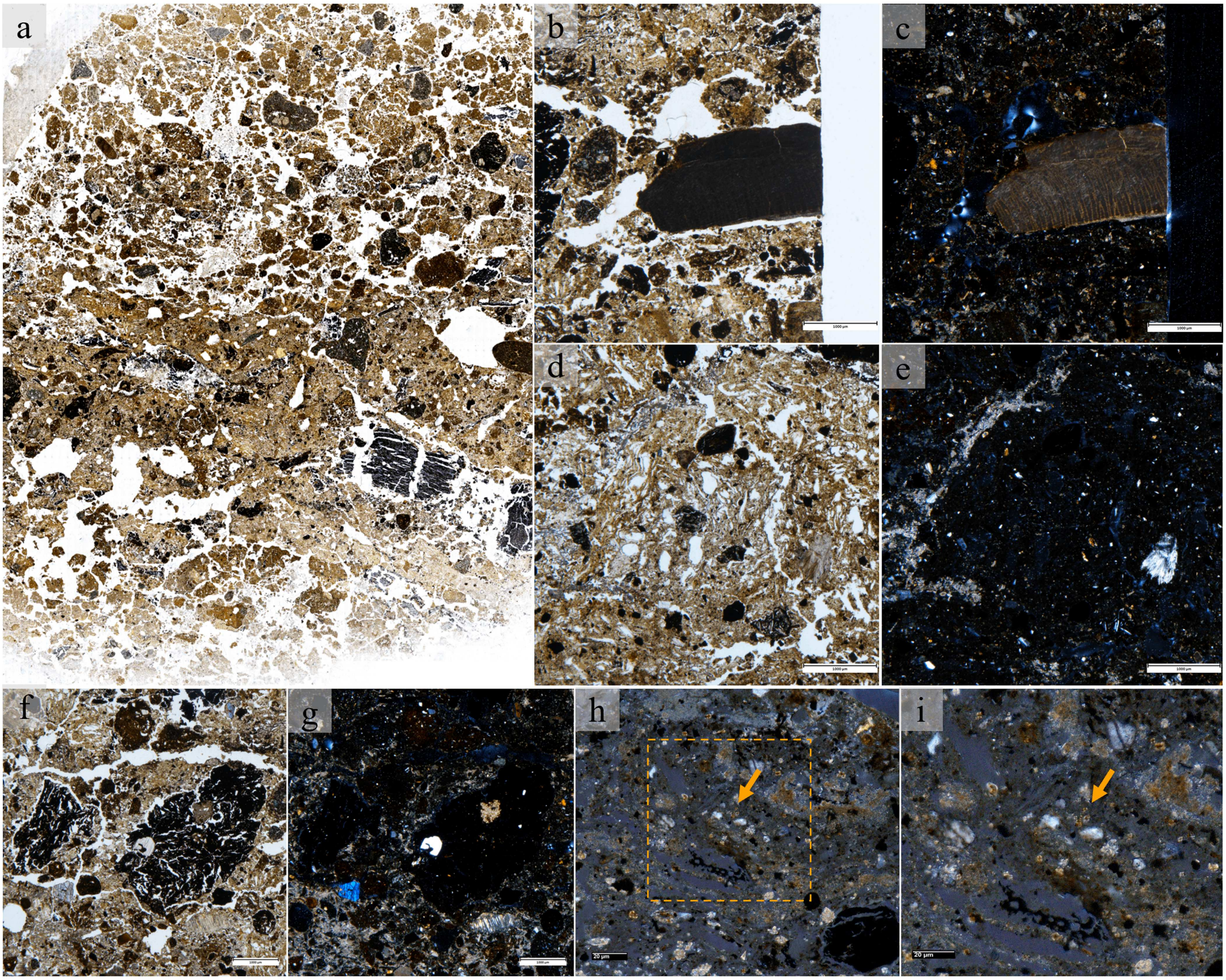

FIGURE 10 | CS 3 (Unit IV) (a) PPL scan of thin section EST-18-1-1b, CS 33, Unit IV. Note the succession of compact clayey sediment (bottom half) and loose trampled sediment (top half). Both contain charcoal and dung remains. Thin section size: 4.5 × 5.5 cm PPL. (b, c) Burnt shell fragment. Note the low birefringence, indicating that aragonite (Figure 6g,h) transformed into calcite due to thermal alteration. PPL and XPL, respectively. Unit IV. (d, e) Unburnt dung fragment. Note its fibrous structure, PPL and XPL, respectively, Unit IV. (f–g) Carbonized dung fragments. PPL and XPL, respectively, Unit IV. (h, i) Burnt fecal spherulites (orange arrow) located inside a partially charred dung fragment. In PPL, they appear blackened. The orange square represents the augmented image area in (i) XPL, Unit IV.

The clay and rounded clastic material have a probable common origin: soil surfaces surrounding the cave, derived from the weathering of pyroclasts and subject to episodic sheetwash and runoff during heavy rains. Another possible clay input mechanism is through percolation from nearby soils through cracks and fissures on the former (fallen) roof cornice. The primary source of weathered volcanic materials is the Teno Massif, found about 10 km upslope from the site. The soils developed on the surface of this massif have been characterized as vertisols. A concentration of rounded basalt gravel observed in Unit III (MFU 21–MFT 11, Figure 8f) could represent an event of high-energy overland flow. The presence of surface crusts (Figure 5e–h) (Mallol and Goldberg 2017; Pagliai and Stoops 2010) in Units VIII, VII, and V indicates that at least during the period of formation of these Units, between the 5th and 7th centuries AD, the cave entrance experienced occasional puddling. In contrast, Units IV–II, which formed under a slightly reduced sheltered area at the cave entrance *after* the major cornice collapse event (Units VI–V) (Figure 4), do not show evidence of puddling. No erosional features or sedimentary discontinuities were observed throughout the sequence.

4.2 | Natural Postdepositional Processes

The entire stratified sequence exhibits spongy and vughy microstructures (Figure 7) that can be explained by the cave's proximity to the ocean and its constant input of salt from exposure to sea spray. Such microstructures are typical of sodic soils, in which aggregate formation and plant growth are hampered by constant sodium-rich salt input and subsequent clay flocculation (Jafarpoor et al. 2021). The presence of limpid clay coatings and partial clay infillings throughout the sequence indicates partial clay mobilization. The abundance of granoporostriated b-fabric, however, likely reflects dispersion processes typical of Na-rich soils, whereby dispersion of the fine fraction allows grains to float and sink within the matrix.

TABLE 4 | Sedimentary depositional rate model, based on the average thickness of each Unit and the average chronological data taken from Hernández et al. (Forthcoming).

Sedimentary depositional rate model							
SU	SU top coordinated cm	Average thickness (cm)	Chronological data (Years BP)	Time span (Years)	SDR (cm/year)	Formation process	Micromorphological interpretation
I	0	20	1451	122	0.164	—	—
II	20	8	1329	34	0.235	Gravitation: – Roofspall Hydric: – Low energy sheetwash Aeloian: – Windblown silt	Incipient soil development
III	28	12	1295	274	0.044	Anthropogenic: – Reworked combustion remains Gravitation: – Roofspall Hydric: – Low energy sheetwash – Episodic moderate energy inwash Aeloian: – Windblown silt	Incipient soil development with reworked wood ash in the top 2 cm
IV	40	13	1021	360	0.036	Anthropogenic: – Combustion structures Gravitation: – Roofspall Hydric: – Low energy sheetwash Aeloian: – Windblown silt	Anthropogenic deposit composed of primary combustion residues (CS2 and CS3) on a geogenic substrate
V	53	6	661	63	0.095	Gravitation: – Roofspall Hydric: – Low energy sheetwash – Stagnant water Aeloian: – Windblown silt	Weakly-developed sodic soil
VI	59	11	598	68	0.162	Gravitation: – Roofspall Hydric: – Low energy sheetwash – Stagnant water	Incipient soil development

(Continues)

Sedimentary depositional rate model							
SU	SU top coordinated cm	Average thickness (cm)	Chronological data (Years BP)	Time span (Years)	SDR (cm/year)	Formation process	Micromorphological interpretation
VII	70	9	530	67	0.134	Aeloian: – Windblown silt Anthropogenic: – Trampled occupation surface(s) Gravitation: – Roofspall Hydric: – Low energy sheetwash	Trampled surface
VIII	79	6	463	54	0.111	Aeloian: – Windblown silt Anthropogenic: – Combustion structure Gravitation: – Roofspall Hydric: – Low energy sheetwash – Stagnant water	Incipient soil development with primary combustion residues (CS1)
IX	85	24	409	242	0.099	Aeloian: – Windblown silt Gravitation: – Roofspall Hydric: – Low energy sheetwash	Incipient soil development
X	109	15	167	91	0.165	Aeloian: – Windblown silt Gravitation: – Roofspall Hydric: – Low energy sheetwash Aeloian: – Windblown silt	Incipient soil development
XI	124	6	76	42	0.143	—	—
XII	130	—	34	—	—	—	—

Sodic soils inhibit water penetration, resulting in poor water absorption and accumulation of stagnant water on the surface. This sodic condition possibly enhanced puddling and the formation of surface crusts as described earlier. Although there are frequent vesicles throughout the sequence, especially in the lower part, these could be associated with water saturation at the subsurface as the deposit accreted. In Tenerife, the development of sodic properties in the local (La Isla Baja) vertisols intensifies with desertification and increased human impact (Quintana et al. 2015; Tejedor et al. 2009). The presence of micromorphological sodic features throughout the Las Estacas sequence, from base to top, suggests that this is a pedogenic process unrelated to anthropogenic impact or arid climatic conditions, and that it might be explained by the proximity of the deposit to the coast.

Stratigraphic Units V and III, formed between the 7th and 13th centuries, exhibit common vertical and horizontal planes (Figure 11a). These reflect the elastic nature of the volcanogenic clay minerals and could be a result of shrink-swell related to sharp changes in atmospheric humidity. The entire sequence is bioturbated, as evidenced by frequent channels filled with fresh rootlets (Figure 11b,c). Authigenic evaporitic crystals were observed in Units IV and III, with higher concentrations in Combustion Structure 3 (Unit IV) (Figure 11d,e,g,h).

The formation and preservation of authigenic evaporites as observed in Units IV–III implies dry sedimentary conditions between the times of Unit IV and the present day (Abdel Aal and Ibrahim 2013; Aquilano et al. 2016; Shahack-Gross and Finkelstein 2008). The combined presence of authigenic evaporites and shrink-swell in the upper part of the sequence (Units IV–II), together with an absence of surface crusts, which are only found from Unit V downwards, and a slight decrease in vesicles and clay illuviation features suggests that generally dryer climatic conditions prevailed at the site until the European conquest (11th–15th centuries). This shift toward increased aridity aligns with the warm and dry conditions characteristic of the "Medieval Climate Anomaly" or the "Medieval Warm Period," a moment in the archipelago marked by demographic growth and intensified exploitation of marine resources (Lécuyer et al. 2021; Mesa 2018; Parker et al. 2020; Santana et al. 2025). However, this pattern does not appear to be homogenous across the islands: in Buenavista, evidence suggests that intensive coastal exploitation can be traced back to the 2nd century, becoming particularly significant from the 5th century onward (Castilla-Beltrán et al. 2025).

Although the Medieval Climate Anomaly roughly coincides with the major cornice collapse event that occurred between Units VI and V, the higher incidence of micromorphological features indicative of wet conditions in Units XII–V than in Units IV–II cannot be explained by the collapse of the roof, since the cave mouth remains largely open even in the interior zone and a substantial difference in internal versus external humidity is not expected. Additional micromorphological samples from the area in front of the cave are needed to test this hypothesis. We expect to observe a similar pattern in those samples, with evidence of higher humidity in the lower Units (up to Unit VI) and drier conditions from Unit V upward.

Regarding possible sources of the evaporites, one is *Tamarix* (tamarisk or salt cedar). This plant contains anhydrite ($CaSO_4$) within its tissues and is adapted to arid or semi-arid saline environments. In Tenerife, *Tamarix canariensis* is typically found in saline soils of the interior and coastal regions, and it is presently found in the vicinity of the cave. The presence of gypsum in the upper part of the sedimentary deposit could be due to Tamarix root growth and degradation in situ. Alternatively, it has been shown that *Tamarix* wood combustion and subsequent hydration of the ashes leads to gypsum formation (Shahack-Gross and Finkelstein 2008; Storey 1994). Therefore, if the occupants of Las Estacas Units IV–II were burning *Tamarix* in the cave, this could also have resulted in postdepositional gypsum formation. In fact, the largest gypsum concentrations are found in association with frequent microscopic combustion residues in CS3. Another possible source of gypsum is seawater, since the cave is permanently exposed to sea spray, and sodic soils in the southern part of Tenerife contain gypsum crystals (Fernández et al. 1982; Moran and Durham 2019; van Vliet et al. 2021). Furthermore, sulfates can also originate from the decomposition of organic matter (Etiégni and Campbell 1991), and microscopic plant and dung residues observed in CS3 provide direct evidence of organic inputs that could have contributed to sulfate formation. Finally, evaporites might have a modern origin, such as gypsum, calcite powder, nitrates, phosphates, and potassium (NPK), which are used as fertilizers and soil flocculators in the nearby plantations. Further research studies are needed to test these hypotheses, including *T. canariensis* burning experiments and assessment of the degree of possible water filtrations from the nearby plantations into the cave.

4.3 | Sediment Deposition Rate

The data presented in the model indicate an SDR average of 0.130 cm/year, peaking in Unit II (0.235 cm/year) and showing the slowest rates at Units IV and III, with 0.036 and 0.044 cm/year, respectively. The other Units maintain a consistent rate between 0.095 and 0.165 cm/year, values that are consistent with slow depositional rates observed in enclosed caves or rock shelters such as Las Estacas.

Micromorphological analysis suggests stratigraphic continuity, as no erosional contacts or features, compositional changes, or evidence of human activity potentially leading to intentional sediment removal (e.g., floor preparation, cleaning, or waste disposal) were observed.

The major cornice collapse event, represented by a mega block between Units VI and V, did not have any visible effect on the sedimentation of Units V–IV at the sampled location, ca. 10 cm inside the current dripline. Nevertheless, a significant chronological gap in radiocarbon dates between Units IV and III has been reported by Hernandez et al. (Forthcoming). Considering the stratigraphic continuity observed in this study, along with the predominantly geogenic nature of the deposit and the anthropogenic nature of the dated material (archaeological bone specimens from Units V and IV), it is plausible that this chronological gap reflects a prolonged occupational hiatus at the site, corresponding to the formation of Units IV and III.

This hiatus in human occupation coincides with the change in the cave's morphology, and it remains unclear to what extent the sediment trap responsible for natural sedimentation persists in the cave's current configuration. Based on these observations, the authors propose three plausible hypotheses to explain the observed features:

1. With the change in the cave's morphology, the natural sediment trap was disrupted, leading to a reduction in the influx of natural sediments into the cavity. As a result, anthropogenic inputs have become the dominant contributors in Units II and I.
2. The change in the cave's morphology did not affect the natural sediment trap. The slower SDR is then explained by a change in anthropogenic input, which played a major role

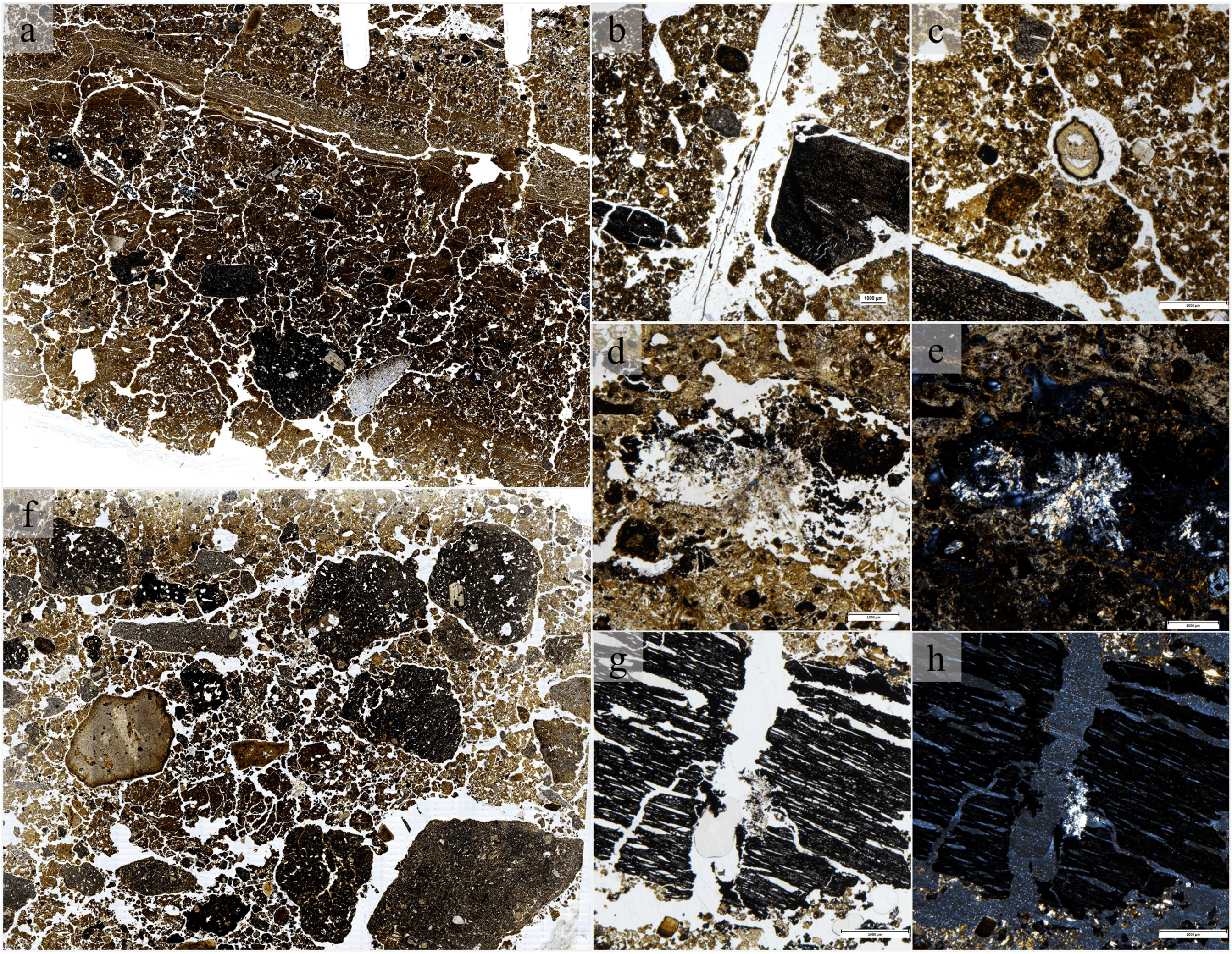

FIGURE 11 | (a) PPL scan of thin section EST-18-1-3, Unit V, PPL. Note the presence of vertical and horizontal planes and moderately developed angular blocky peds from incipient aggregation from shrink-swelling. Thin section size: 4.5 x 5.5 cm. (b, c) Root remains partially filling channels. PPL, Unit VIII. (d, e) Formation of authigenic evaporitic crystals mixed with unidentified charred material, PPL and XPL respectively. Unit IV. (f) PPL scan of thin section EST-18-3-4a, Unit III, PPL. Note the concentration of rounded basalt fragments, indicating a high-energy depositional event. Thin section size: 4.5 × 5,5 cm. (g, h) Evaporitic crystal in a charcoal fragment, PPL and XPL respectively, Unit IV.

in sedimentary accretion. At the microscopic scale, the deposits remain predominantly natural (geogenic), but the decrease in SDR in Units IV and III reflects a reduction in human activity, while natural sedimentation remained constant. The peak in Unit II, followed by a return to the average rate in Unit I, suggests re-occupation of the site at the initially higher intensity rate, before settling back to the average rate. The anthropogenic factor involves intentional and unintentional input of materials as well as trampling.

3. The change in the cave's morphology did not alter the sediment trap, but it triggered a small landslide that displaced an unknown amount of sediment dating from the start of the occupation until 1100–1200 AD. These sediments, together with their associated archaeological materials, are currently found downslope a few meters from the cave (Hernández et al. Forthcoming, Figure 3c).

Testing any of these hypotheses is currently challenging. Unit I was fully excavated during the 1990s excavations (Galván et al. 1998), and micromorphology samples of Unit II only encompass 2–3 cm at the contact with Unit III. Further research studies are needed, including systematic sampling across the site and especially in Unit IV (from which only combustion structures were sampled), comprehensive excavation of the lower layers (Units VIII–XII), along with a geomorphological reconstruction of the cave prior to its partial collapse.

4.4 | Human Activities

Microscopic evidence of human activity is observed primarily in the combustion remains (Units VIII, IV, and III) and in Unit VII (trampled layer). Microscopic remains linked to human activity are surprisingly scarce, compared with the abundance recorded in the 1990s excavation (Table 2). Microscopic lithic remains were observed, but there is no clear distinction between the natural spall of the cave's roof and walls and the remains of basalt knapping. The contrast between the density of the macroscopic and microscopic records can be explained by a low incidence of fracture and dispersion from trampling, which might in turn be related to low-intensity occupations. The macroscopic record is well preserved, with numerous ceramic shards and bones found complete and in situ (see Figures 10, 11, and 12 in Galván et al. 1998).

Micromorphological evidence of trampling was only observed in Unit VII, which is composed of loose aggregates with a dominant complex packing void microstructure and secondary channels. Trampling is manifested in the deformation, breakage, and reorientation of aggregates, as well as in the compaction of the voids, indicating repeated movement of people across the surface under dry conditions (Gé et al. 1993). The variety and abundance of aggregates (Figure 8) suggest a high intensity of occupation.

Combustion structures constitute the primary evidence of human activity at the site. CS1 (Unit VIII) has a black layer composed of silt and fine sand-sized charred plant matter and charcoal in a clay geogenic groundmass. A 1 cm-wide patch of recrystallized ash is observed at the top of the structure, cutting through the surface crust. This substrate is consistent with a simple hearth (Mallol et al. 2013). This microstratigraphic succession suggests that surface water reworked a primary combustion structure, translocating and locally redepositing the charred materials. This erosional event is further evidence of the generally moist and wet conditions prevailing at the cave entrance zone during the formation of the lower part of the Las Estacas sequence.

CS2, in Unit IV, is composed of a millimeter-thin red layer overlain by a rich calcitic-ash deposit of approximately. 5.5–6 cm. Two distinct MFUs constitute CS2: MFU 16 and MFU 17, containing common and abundant rubified clay aggregates, respectively. These aggregates may have derived from the use of local shrub vegetation as fuel, including entire plants with attached roots and soil particles, as previously proposed for similar features in other archaeological wood ash deposits (Meignen et al. 2017).

Three distinct combustion episodes can be distinguished in CS2. The first combustion episode is observed from the base to a thin bed of sand-sized rubified rounded basalts. Up to five successive layers of crusted ashes were observed within this first combustion episode, indicating at least five re-lighting moments. Between the rubified bedded sand-sized basalts and MFU 17, a clear crust of ash can be observed, with very well-preserved calcite pseudomorphs, spanning almost the entirety of the thin section. Three additional layers of crusted ashes can be observed in MFU 16, indicating three additional lighting episodes (Figure 9c,d). The presence of possible sintered ash layers, partially or totally isotropic (Figure 10e,f) intertwined with the crusted layers and the absence of charcoal fragments suggest consistent high-temperature well-oxidized burning ranging from 600°C to 800°C (Canti 2017; Karkanas 2021). No food waste, ceramic, lithic, or any other anthropogenic microscopic remains that could point to possible activities carried out around the fire were observed. MFU 17, the top of the combustion feature, is interpreted as the third re-lighting event, where more fuel is added without a previous selection and cleaning, tossing bushes and entire plants with soil particles attached to them.

CS3, also in Unit IV and directly on top of CS2, is composed of MFUs 18, 19, and 20. The absence of a red/black layer in the combustion structure, as well as the mixture between burnt and unburnt elements in MFU 18 and 20, suggests intensive trampling, altering its initial morphology and microstructure, and mixing the burning residue and combusted material with the unaltered remains of the substrate. Also, the ubiquitous presence of charcoal fragments and the different states of thermal alteration shown by the dung and clayey aggregates suggest irregular and low-temperature burning.

Combustion remains in the shape of reworked ash mixed with clay and volcanic clasts, and is found in the top cm of Unit III, in contact with Unit II. The lack of integrity in the deposit and the mixture with the geogenic deposit indicate that it is reworked, possibly swept inside the cave. The wood ash is possibly associated with a combustion structure located in the Unit III-II contact reported from the 1990s excavation (See Table 1 in Galván et al. 1998; Hernández, personal communication).

Overall, microscopic traces of human activity at Las Estacas are scarce. Only three out of the eight sampled Units (VIII, IV, and III) possess clear indicators of human activity: combustion structures and heavily trampled surfaces. In situ cave occupation surfaces are absent. Ash and material preservation vary according to depth and humidity: materials in the lower part of the sequence (Units IX–V) are less preserved (e.g., recrystallized ash patch in CS1), while micro remains in the topmost Units (IV–II) are best preserved.

Our evidence indicates a low human impact at the sampled locations, in contrast to the rich archaeological record reported by Galván et al. (1999). Given the small size of the interior cave space at these sampled locations, it may have functioned primarily as a zone for fire-making and refuse disposal rather than as heavily trampled occupation surfaces. Further investigation of the cave porch area, currently buried beneath roof spall, as well as of the possible continuity between Las Estacas 1 and 2 prior to the cornice collapse, will be necessary to evaluate this hypothesis. Settlement patterns documented at nearby sites, such as Las Fuentes and Las Arenas, where domestic and funerary contexts coexisted, provide broader contextual support for this interpretation (Galván et al. 1991, 1999).

5 | Conclusions

This micromorphological study of Las Estacas cave has contributed information about the nature of the sedimentary sequence and its associated natural and anthropogenic depositional and postdepositional dynamics. The findings offer significant clues about the local environmental conditions that prevailed at the site during the formation of the deposits and enable us to assess the impact of human occupation, as well as to identify specific periods of relatively high occupation intensity. Furthermore, it is an example of low anthropogenic impact with predominant natural sedimentation and sodic vertisol formation.

The main agents of sedimentation at the cave are low-energy surface flow, gravity, and the wind, resulting in a combination of autochthonous roof spall and detrital fines from the surrounding soils. The sediment underwent pedogenesis and developed sodic vertisol properties due to the cave's proximity to the seashore and the constant exposure to sea spray. The entire studied sequence shows stratigraphic continuity, with the bottom layers consisting of features that suggest humid conditions and frequent puddling inside the cave, and a change toward more arid climatic conditions from Unit IV onwards.

The sedimentary depositional rate model indicates a continuous, slow deposition related to closed dynamics such as caves, showing a sharp decrease in the depositional rate that coincides with the occupational hiatus. The dynamic postdepositional environment revealed through micromorphology, with recurrent shrink-swell, clay translocation, and authigenic crystal growth and bioturbation, may have caused reworking at the microscopic and molecular level. This should be taken into account in the study of phytoliths, pollen, lipid biomarkers, and ancient DNA from the site.

This site formation investigation has highlighted the flexibility and adaptability required for human occupation of island settings. First, we show that Las Estacas Cave, located at a rough spot directly exposed to the North winds and ocean spray, was continuously occupied by indigenous people from the time of the earliest settlers up until the arrival of Europeans. Second, our data indicate that there was continuous occupation despite environmental change towards drier conditions. Third, the presence of ovicaprine dung mixed with domestic residues speaks of mixed coastal subsistence strategies.

Further investigations are necessary to explore the spatial distribution of human activity in and around the cave before and after the roof collapse event. The sparse microscopic anthropogenic signal, contrasted with abundant field evidence, suggests that throughout the sequence, human activity was concentrated at the cave entrance, while the interior was mainly used for fire-related activities and experienced minimal trampling-derived sedimentation.

The results of this study contribute to advancing debates on pre-European behavior and activities associated with domestic archaeological contexts in the Canary Islands and, more generally, on human subsistence in islands. Finally, this study illustrates the high potential of the microstratigraphic approach as a tool for site formation and paleoenvironmental research.

Author Contributions

Pedro García-Villa: conceptualization, investigation, writing – original draft, methodology, visualization, software, formal analysis. **Cristo M. Hernández:** resources, writing – review and editing, supervision, project administration, funding acquisition. **Carolina Mallol:** conceptualization, validation, resources, data curation, writing – review and editing, supervision, project administration, funding acquisition.

Acknowledgments

This article is part of P. García-Villa's PhD thesis, and all authors agree. The authors would like to thank Álvaro Castilla-Beltrán for his insight on the chronology of the site. Our gratitude goes to all those involved in the excavation and research process; this study would not have been possible without their commitment, skill, and generous teamwork. The authors would also like to thank the anonymous reviewers for their valuble comments and suggestions, which helped improve this research article. This research was funded by a predoctoral contract awarded to PGV in the framework of the "Initium ULL" contracts, co-funded by the Universidad de La Laguna and the Consejería de Universidades, Ciencia e Innovación y Cultura. The project has received funding from the "María Rosa Alonso" program of the Universidad de La Laguna and from the PALEOCAN project (ID: 2018PATRI19), co-financed by the Cabildo de Tenerife, Fundación CajaCanarias, and Fundación "la Caixa."

Data Availability Statement

Data that support the findings of this study are available from the corresponding author upon reasonable request.

References

Abdel Aal, T. S., and A. M. Ibrahim. 2013. "Studies on the Micromorphology of Salt-Affected Soils from El-Fayoum Depression, Egypt." In *Developments in Soil Classification, Land Use Planning and Policy Implications: Innovative Thinking of Soil Inventory for Land Use Planning and Management of Land Resources*, edited by S. A. Shahid, F. K. Taha, and M. A. Abdelfattah, 373–392. Springer Netherlands.

Abdel-Monem, A., N. D. Watkins, and P. W. Gast. 1972. "Potassium-Argon Ages, Volcanic Stratigraphy, and Geomagnetic Polarity History of the Canary Islands; Tenerife, La Palma and Hierro." *American Journal of Science* 272, no. 9: 805–825.

Anguita, F., C. Fernández, Á. Márquez, R. León, and R. Casillas. 2025. "The Canary Hotspot Revisited: Refutation of the Hawaii Paradigm and an Alternative, Plate-Based Hypothesis." *Earth-Science Reviews* 261: 105038.

Aquilano, D., F. Otálora, L. Pastero, and J. M. García-Ruiz. 2016. "Three Study Cases of Growth Morphology in Minerals: Halite, Calcite and Gypsum." *Progress in Crystal Growth and Characterization of Materials* 62, no. 2: 227–251.

del Arco, M., M. del-Arco-Aguilar, C. Benito-Mateo, and C. Rosario-Adrián, eds. 2016. *Un taller romano de púrpura en los límites de la Ecúmenes. Lobos 1 [Fuerteventura—Islas Canarias]. Primeros resultados.* Museo Arqueológico de Tenerife.

Armas-Espinel, S., J. M. Hernández-Moreno, R. Muñoz-Carpena, and C. M. Regalado. 2003. "Physical Properties of 'Sorriba'-Cultivated Volcanic Soils From Tenerife in Relation to Andic Diagnostic Parameters." *Geoderma* 117, no. 3–4: 297–311.

Arnay, M., and E. G. Reimers. 1984. "Vasos cerámicos prehispánicos de Tenerife: un análisis estadístico." *Anuario de Estudios Atlánticos* 1, no. 30: 79–107.

Blaauw, M., and J. A. Christen. 2011. "Flexible Paleoclimate Age-Depth Models Using an Autoregressive Gamma Process." *Bayesian Analysis* 6, no. 3: 457–474.

Canti, M. 2017. "Charred Plant Remains." In *Archaeological Soil and Sediment Micromorphology*, edited by C. Nicosia and G. Stoops, 141–142. Wiley-Blackwell.

Carracedo, J. C. 1979. *Paleomagnetismo e historia volcanica de Tenerife.* Cabildo de Tenerife.

Castilla-Beltrán, A., E. Fernández-Palacios, L. de Nascimento, et al. 2025. "Shell Middens and Soil Terraces as Archives of Human-Littoral Interactions Since the First Settlement of Northwestern Tenerife, the Canary Islands." *Holocene* 36, no. 3: 299–311. https://doi.org/10.1177/09596836251396065.

Courty, M.-A. 2001. "Microfacies Analysis Assisting Archaeological Stratigraphy." In *Earth Sciences and Archaeology*, edited by P. Goldberg, V. T. Holliday, and C. Reid Ferring, 205–239. Springer US.

Descripción de las Unidades Geológicas de Tenerife. 2010. Grafcan. https://www.grafcan.es/.

Etiégni, L., and A. G. Campbell. 1991. "Physical and Chemical Characteristics of Wood Ash." *Bioresource Technology* 37, no. 2: 173–178.

Fernández, E., M. Tejedor, and P. Quantin. 1982. *Suelos de regiones volcánicas. Tenerife, Islas Canarias*. Universidad de La Laguna.

Fernández, E., and M. L. Tejedor. 1975. "Andosoles Canarios. I. Características generales de estos suelos." *Anales de Edafología y Agrobiología* 34, no. 3–4: 1975.

Fernández-Caldas, E., C. Rodríguez-Pasucal, and C. Rodríguez. 1980. "Vertisoles formados sobre materiales volcánicos (Islas Canarias). Typic Pellusterts. Características morfológicas, fisico-químicas y mineralógicas. Interpretación y clasificación." *Anales de Edafología y Agrobiología* 39, no. 7–8: 1443–1460.

Fernández-Palacios, E., A. Castilla-Beltrán, G. Simon-Pierre, et al. Forthcoming. "Deciphering Indigenous Lifeways at Buracas (La Palma, Canary Islands) From an Integrated Multi-Method Perspective." *African Archaeological Review*.

Fernández-Palacios, E., A. V. Herrera-Herrera, S.-P. Gilson, et al. 2023a. "Distinguishing Between Sheep and Goat in Archaeological Fumiers Through Faecal Lipid Biomarkers: The Case of Belmaco Cave (Canary Islands, Spain)." *Quaternary International: The Journal of the International Union for Quaternary Research* 683–684: 135–144. https://doi.org/10.1016/j.quaint.2023.08.012.

Fernández-Palacios, E., M. Jambrina-Enríquez, S. M. Mentzer, et al. 2023b. "Reconstructing Formation Processes at the Canary Islands Indigenous Site of Belmaco Cave (La Palma, Spain) Through a Multiproxy Geoarchaeological Approach." *Geoarchaeology* 38, no. 6: 713–739. https://doi.org/10.1002/gea.21972.

Flores, C., J. M. Larruga, A. M. González, M. Hernández, F. M. Pinto, and V. M. Cabrera. 2001. "The Origin of the Canary Island Aborigines and Their Contribution to the Modern Population: A Molecular Genetics Perspective." *Current Anthropology* 42, no. 5: 749–755.

Fregel, R., A. C. Ordóñez, J. Santana-Cabrera, et al. 2019. "Mitogenomes Illuminate the Origin and Migration Patterns of the Indigenous People of the Canary Islands." *PLoS One* 14, no. 3: e0209125.

Galván, B., V. Alberto, C. M. Hernández, et al. 1998. Excavaciones arqueológicas en las Cuevas de Las Estacas (Buenavista del Norte, Tenerife). *XIII Coloquio de Historia Canario-Americana*. http://coloquioscanariasamerica.casadecolon.com/index.php/CHCA/article/view/8249/7323.

Galván, B., M. Arnay, J. Carracedo, et al. 1991. *La cueva de Las Fuentes (Buenavista del Norte-Tenerife)*. Museo Arqueologico de Tenerife.

Galván, B., C. M. Hernández, V. A. Barroso, et al. 1999. Poblamiento prehistórico en la costa de Buenavista del Norte (Tenerife). El conjunto arqueológico Fuente-Arenas. Investigaciones Arqueologicas.

Galván, B., M. C. Hernández Gómez, C. M. García Ávila, et al. 2004. Los concheros de La Fuente: consideraciones metodológicas y resultados preliminares. https://riull.ull.es/xmlui/handle/915/18609.

Gé, T., M. A. Courty, W. Matthews, and J. Wattez. 1993. "Sedimentary Formatoin Processes of Occupation Surfaces." In *Formation Processes in Archaeological Contexts*, edited by P. Goldberg, D. T. Nash, and Petraglia, 149–163. Prehistory Press.

Gómez, D., J. de León, J. F. Navarro, E. Marrero, I. Abreu, and J. Cuenca. 2014. La micromorfología de suelos en contexto arqueológico. Una aplicación en el Archipiélago Canario: Fiquinineo - Peña de las Cucharas (Teguise, Lanzarote). *XX Coloquio de Historia Canario-Americana*. https://dialnet.unirioja.es/servlet/articulo?codigo=7341656.

Hernández, C. M., A. Castilla, J. Santana, et al. Forthcoming. "The First Human Settlement of Tenerife, Canary Islands. New Data From Las Estacas Cave (Buenavista del Norte)." *Journal of Island and Coastal Archaeology*.

Hernández, C. M., E. Marrero, and M. Arnay. 2024. *Patrimonio Arqueológico de Canarias. Tenerife*. Identitaria Canarias.

Herrera-Herrera, A. V., H. Padrón-Herrera, E. Iriarte, V. Alberto-Barroso, M. A. Moreno-Benítez, and C. Mallol. 2024. "Fecal Biomarkers and Micromorphological Indicators of Sheep Penning and Flooring at La Fortaleza Pre-Hispanic Site (Gran Canaria, Canary Islands)." *IScience* 27, no. 3: 109171.

Jafarpoor, F., S. Manafi, and R. M. Poch. 2021. "Textural Features of Saline-Sodic Soils Affected by Urmia Lake in the Northwest of Iran." *Geoderma* 392: 115007.

Karkanas, P. 2021. "All about Wood Ash: Long Term Fire Experiments Reveal Unknown Aspects of the Formation and Preservation of Ash With Critical Implications on the Emergence and Use of Fire in the Past." *Journal of Archaeological Science* 135: 105476.

Lécuyer, C., J. Goedert, J. Klee, et al. 2021. "Climatic Change and Diet of the Pre-Hispanic Population of Gran Canaria (Canary Archipelago, Spain) During the Medieval Warm Period and Little Ice Age." *Journal of Archaeological Science* 128: 105336.

Mallol, C., and P. Goldberg. 2017. "Cave and Rock Shelter Sediments." In *Archaeological Soil and Sediment Micromorphology*, edited by C. Nicosia and G. Stoops, 359–381. John Wiley & Sons, Ltd.

Mallol, C., C. M. Hernández, D. Cabanes, et al. 2013. "The Black Layer of Middle Palaeolithic Combustion Structures. Interpretation and Archaeostratigraphic Implications." *Journal of Archaeological Science* 40, no. 5: 2515–2537.

Meignen, L., P. Goldberg, and O. Bar-Yosef. 2017. "Together in the Field: Interdisciplinary Work in Kebara and Hayonim Caves (Israel)." *Archaeological and Anthropological Sciences* 9, no. 8: 1603–1612.

Menéndez, I., J. L. Díaz-Hernández, J. Mangas, I. Alonso, and P. J. Sánchez-Soto. 2007. "Airborne Dust Accumulation and Soil Development in the North-East Sector of Gran Canaria (Canary Islands, Spain)." *Journal of Arid Environments* 71, no. 1: 57–81.

Mesa, E. M. 2018. *Entre lapas y burgados. Los Guanches y el aprovechamiento de los recursos marisqueros*. Fundacion CajaCanarias.

Mizota, C., and Y. Matsuhisa. 1995. "Isotopic Evidence for the Eolian Origin of Quartz and Mica in Soils Developed on Volcanic Materials in the Canary Archipelago." *Geoderma* 66, no. 3–4: 313–320. https://doi.org/10.1016/0016-7061(95)00004-8.

Mora, I. 2021. "La dispersión de la escritura Líbico-Bereber desde Numidia hasta Canarias." In *Aprender la escritura, olvidar la escritura. Nuevas perspectivas sobre la historia de la escritura en el Occidente romano*, edited by N. Moncunill and M. Ramírez-Sanchez. Universidad del País Vasco.

Morales, J., C. Speciale, A. Rodríguez-Rodríguez, et al. 2026. "Agriculture and Crop Dispersal in the Western Periphery of the Old World: The Amazigh/Berber Settling of the Canary Islands (ca. 2nd–15th Centuries Ce)." *Vegetation History and Archaeobotany* 35: 219–233. https://doi.org/10.1007/s00334-023-00920-6.

Moran, M. A., and B. P. Durham. 2019. "Sulfur Metabolites in the Pelagic Ocean." *Nature Reviews Microbiology* 17: 665–678.

Muhs, D. R., J. Meco, J. R. Budahn, G. L. Skipp, J. F. Betancort, and A. Lomoschitz. 2019. "The Antiquity of the Sahara Desert: New Evidence From the Mineralogy and Geochemistry of Pliocene Paleosols on the Canary Islands, Spain." *Palaeogeography, Palaeoclimatology, Palaeoecology* 533: 109245.

Nicosia, C. and Stoops, G., eds. 2017. *Archaeological Soil and Sediment Micromorphology*. Wiley-Blackwell.

Pagliai, M., and G. Stoops. 2010. "19—Physical and Biological Surface Crusts and Seals." In *Interpretation of Micromorphological Features of Soils and Regoliths*, edited by G. Stoops, V. Marcelino, and F. Mees, 419–440. Elsevier.

Parker, W., Y. Yanes, E. Mesa Hernández, et al. 2020. "Shellfish Exploitation in the Western Canary Islands Over the Last Two Millennia." *Environmental Archaeology* 25, no. 1: 14–36.

Quintana, S. C., C. L. Verna, M. K. T. Salguero, et al. 2015. "Dealing With Desertification in the Canary Islands: A Strategic Planning Methodology for Complex Problematiques." *Journal of Economics, Business and Management* 2: 33–54.

Rodríguez, A., J. Santana Cabrera, P. Castellano Alonso, et al. 2021. "Un lugar entre las dunas. Aprovechamiento oportunista de un espacio costero durante la etapa preeuropea de la isla de Gran Canaria (circa siglos VIII–XI AD)." *Trabajos de Prehistoria* 78, no. 2: 325–343.

Santana, J., M. Del Pino, J. Morales, et al. 2024. "The Chronology of the Human Colonization of the Canary Islands." *Proceedings of the National Academy of Sciences* 121, no. 28: e2302924121.

Santana, J., M. Del Pino Curbelo, E. Iriarte, et al. 2025. "Climate, Biogeography, and Human Resilience in the Demographic History of the Canary Islands During the Amazigh Period." *Scientific Reports* 15: 19485. https://doi.org/10.1038/s41598-025-04302-y.

Serrano, J. G., A. C. Ordóñez, J. Santana, et al. 2023. "The Genomic History of the Indigenous People of the Canary Islands." *Nature Communications* 14, no. 1: 4641.

Shahack-Gross, R., and I. Finkelstein. 2008. "Subsistence Practices in an Arid Environment: A Geoarchaeological Investigation in an Iron Age Site, the Negev Highlands, Israel." *Journal of Archaeological Science* 35, no. 4: 965–982.

Springer, R. A. 2015. La escritura Líbico-Bereber de las Islas Canarias: ¿uno o varios alfabetos? Tabona.

Stoops, G. 2021. *Guidelines for Analysis and Description of Soil and Regolith Thin Sections*, 2nd ed. Wiley. https://doi.org/10.1002/9780891189763.

Storey, R. 1994. "An X-Ray Microanalysis Study of the Salt Glands and Intracellular Calcium Crystals of Tamarix." *Annals of Botany* 73, no. 3: 307–313.

von Suchodoletz, H., B. Glaser, T. Thrippleton, et al. 2013. "The Influence of Saharan Dust Deposits on La Palma Soil Properties (Canary Islands, Spain)." *Catena* 103: 44–52.

Tejedor, M., C. Jiménez, S. Armas-Espinel, and J. M. Hernández-Moreno. 2009. "Classification of Anthropogenic Soils With Andic Properties." *Soil Science Society of America Journal* 73, no. 1: 170–175.

Tomé, L., M. Jambrina-Enríquez, N. Égüez, et al. 2022. "Fuel Sources, Natural Vegetation and Subsistence at a High-Altitude Aboriginal Settlement in Tenerife, Canary Islands: Microcontextual Geoarchaeological Data From Roques de García Rockshelter." *Archaeological and Anthropological Sciences* 14, no. 10: 195.

Troll, V., and Carracedo, J.. 2016a. "The Geology of Tenerife." In *The Geology of the Canary Islands*, edited by V. Troll and J. Carracedo, 227–355. Elsevier.

Troll, V., and Carracedo, J.. 2016b. *The Geology of the Canary Islands*. Elsevier Science Publishing.

van Vliet, D. M., F. A. B. von Meijenfeldt, B. E. Dutilh, et al. 2021. "The Bacterial Sulfur Cycle in Expanding Dysoxic and Euxinic Marine Waters." *Environmental Microbiology* 23, no. 6: 2834–2857.

Yanes, M., C. del, B. Galván, and C. M. Hernández. 2001. "El uso de la madera en yacimientos arqueológicos del NW de Tenerife. Contribución del antracoanálisis." *Anuario Del Instituto de Estudios Canarios* 363: 383.

Supporting Information

Additional supporting information can be found online in the Supporting Information section.

Supporting File 1: gea70063-sup-0001-Appendix_1_Photogrammetry_Estacas_1_V2.pdf.
Supporting File 2: gea70063-sup-0002-Appendix_2_MFUs.pdf.
Supporting File 3: gea70063-sup-0003-FOR_REVIEW_Appendix_3_Table_with_abundancies_per_MFU.xlsx.